

1 **C/EBP δ -induced epigenetic changes control the dynamic**
2 **gene transcription of S100A8 and S100A9**

3

4 **Saskia-L. Jauch-Speer¹, Jonas Wolf¹, Marisol Herrera-Rivero², Leonie**
5 **Martens^{1,2}, Achmet Imam Chasan¹, Anika Witten², Birgit Markus³, Bernhard**
6 **Schieffer³, Thomas Vogl¹, Monika Stoll^{2,4}, Johannes Roth^{1,5} and Olesja Fehler¹**

7

8 ¹Institute of Immunology, University of Münster, 48149 Münster, Germany

9 ²Institute of Human Genetics, Genetic Epidemiology, University of Münster, 48149 Münster,
10 Germany

11 ³Clinic for Cardiology, Angiology and Internal Intensive Medicine, University Hospital
12 Marburg, 35043 Marburg, Germany

13 ⁴CARIM Cardiovascular Research School, Dept. of Biochemistry, Genetic Epidemiology and
14 Statistical Genetics, Maastricht University, 6229 ER Maastricht, The Netherlands

15 ⁵Lead contact and Corresponding author: rothj@uni-muenster.de

16

17 **SUMMARY**

18 The proinflammatory alarmins S100A8 and S100A9 are among the most abundant proteins
19 in neutrophils and monocytes but completely silenced after differentiation to macrophages.
20 The molecular mechanisms of the extraordinarily dynamic transcriptional regulation of
21 *s100a8* and *s100a9* genes, however, are only barely understood. Using an unbiased
22 genome-wide CRISPR/Cas9 knockout based screening approach in immortalized murine
23 monocytes we identified the transcription factor C/EBP δ as a central regulator of S100A8
24 and S100A9 expression. *S100a8* and *S100a9* expression was further controlled by the
25 C/EBP δ -antagonists ATF3 and FBXW7. We confirmed the clinical relevance of this
26 regulatory network in subpopulations of human monocytes in a clinical cohort of
27 cardiovascular patients. Moreover, we identified specific C/EBP δ -binding sites within *s100a8*
28 and *s100a9* promoter regions, and demonstrated that C/EBP δ -dependent JMJD3-mediated
29 demethylation of H3K27me₃ is indispensable for their expression. Overall, our work
30 uncovered C/EBP δ as a novel regulator of S100A8 and S100A9 expression. Therefore,
31 C/EBP δ represents a promising target for modulation of inflammatory conditions that are
32 characterised by S100A8 and S100A9 overexpression.

33 **ABBREVIATIONS**

34 ATAC-seq = Assay for Transposase-Accessible Chromatin using sequencing; ATF3 =
35 activating transcription factor 3; C/EBP β/δ = CCAAT/Enhancer-Binding-Protein β/δ ; CAD =
36 coronary artery disease; Cas9 = CRISPR associated protein 9; cDNA = complementary
37 DNA; ChIP = chromatin immunoprecipitation; COX-2 = cyclooxygenase-2;
38 CRISPR=clustered regularly interspaced short palindromic repeats; DAMPs=danger-
39 associated molecular patterns; FBXW7 = F-Box And WD Repeat Domain Containing 7;
40 GeCKO = Genome-Scale CRISPR/Cas9 Knockout; GFP = green fluorescent protein; GM-
41 CSF= granulocyte-macrophage colony-stimulating factor; IL-6 = Interleukin-6; IRF7 =
42 interferon regulatory factor 7; JMJD3 = JmjC Domain-Containing Protein 3; KLF5 = krüppel-
43 like factor 5; KO = Knockout; LPS = lipopolysaccharide; MaGECK = Model-based Analysis of
44 Genome-wide CRISPR-Cas9 Knockout; MI = myocardial infarction; MSCV = murine stem
45 cell virus; MRP8/14 = myeloid-related protein 8/14; NGS = Next-generation Sequencing;
46 qRT-PCR = Quantitative reverse transcription polymerase chain reaction; RA = rheumatoid
47 arthritis; ROS = reactive oxygen species; RRA = robust rank aggregation; STAT3 = signal
48 transducer and activator of transcription 3; TLR4 = toll-like receptor 4; TNF- α = tumor
49 necrosis factor- α ; TRE = Tet Response Element; WT = wildtype;

50

51 **KEYWORDS**

52 C/EBP δ ;Calprotection;CRISPR/Cas9 screen;monocytes;S100A8/A9

53 INTRODUCTION

54 As the first line of immune defense, both, monocytes and neutrophils are important for the
55 modulation of the innate immune response. To amplify the immune response at sites of
56 inflammation, the activation of further immune cells is required, mediated by the release of
57 signaling molecules such as chemokines and DAMPs (damage-associated molecular
58 patterns). The two members of the S100 family, S100A8 and S100A9, also termed myeloid-
59 related proteins 8 and 14 (MRP8 and MRP14), respectively, belong to the group of DAMPs
60 or so-called alarmins. Their primary expression is referred to myeloid-lineage derived cells,
61 particularly neutrophils and monocytes, where S100A8 and S100A9 are predominantly
62 present as a heterodimeric complex, also called calprotectin (Austermann, Spiekermann and
63 Roth, 2018).

64 Intracellularly, S100A8/S100A9 complexes represent up to 40% of the soluble protein
65 content in neutrophils and about 5% in monocytes (Hessian, Edgeworth and Hogg, 1993).
66 However, in mature macrophages, protein and mRNA expression of these factors is
67 completely downregulated. This data indicates that expression of S100A8 and S100A9 is
68 controlled by the most dynamic promoters in myeloid cells. The S100A8/A9 complex
69 interacts with the cytoskeleton in a calcium-dependent manner. Calcium-induced
70 (S100A8/A9)₂ tetramer promotes tubulin polymerization and microtubule bundling, thereby
71 affecting transendothelial migration of phagocytes (Leukert *et al.*, 2006). During inflammation
72 or tissue damage S100A8/A9 is actively secreted by neutrophils and monocytes, and
73 represents the most abundant DAMP/alarmin activating inflammatory processes in infection,
74 cancer, autoimmunity and cardiovascular diseases. The S100A8/A9 complex is recognized
75 by Toll-like receptor 4 (TLR4), which leads to the production of proinflammatory cytokines
76 and chemokines (Fassl *et al.*, 2015). Accordingly, S100A9 KO mice exhibit decreased
77 pathogenic outcomes in several mouse models of disease, such as sepsis (Vogl *et al.*,
78 2007), autoimmune disease (Loser *et al.*, 2010) or arthritis (Van Lent *et al.*, 2008). In
79 addition, S100A8 and S100A9 are highly abundant during infectious diseases and exhibit

80 anti-microbial activities. The S100A8/A9 complex plays a crucial role in host defense against
81 bacterial and fungal pathogens by sequestering manganese and zinc ions which compete
82 with high affinity bacterial transporters to import these essential nutrient metals (Kehl-Fie and
83 Skaar, 2010; Kehl-Fie *et al.*, 2011). In contrast to the proinflammatory role of S100A8/A9,
84 also regulatory functions in terms of hyporesponsiveness in phagocytes, resembling a
85 classical endotoxin-induced tolerance, have been described (Freise *et al.*, 2019).

86 In humans, S100A8/A9 is the most abundant alarmin in many clinically relevant diseases,
87 and is closely associated with disease activity in rheumatoid arthritis, inflammatory bowel
88 disease, sepsis, cardiovascular diseases, multiple sclerosis, acute lung injury and psoriasis
89 (Foell *et al.*, 2004). Altered S100A8/A9 expression has also been found in different cancer
90 types, including gastric, colorectal, breast, lung, prostate and liver cancer (Cross *et al.*,
91 2005). Despite the high expression in neutrophils and monocytes under inflammatory
92 conditions, and the strong effects of S100A8 and S100A9 on disease activities,
93 transcriptional mechanisms regulating these extreme dynamics of gene expression remain
94 unclear. Identifying the mechanisms regulating S100A8 and S100A9 gene expression may
95 open new insights into the pathological processes involving S100A8/A9 during inflammatory
96 conditions.

97 So far, several potential transcription factors modulating S100A8 and S100A9 expression
98 have been described (Kuruto-Niwa *et al.*, 1998; Fujii, Manabe and Nagai, 2011; Lee *et al.*,
99 2012; Liu *et al.*, 2016; Yang *et al.*, 2017), but their functional relevance remains unresolved.
100 Many of the stated studies used malignant immortalized cell lines or even cell models whose
101 homologous primary cells do not express these genes at all.

102 To overcome difficulties of artificial expression and malignant cell lines we used ER
103 (estrogen-regulated) Hoxb8 cells, estrogen dependent transiently immortalized myeloid
104 precursor cells that can be differentiated to primary monocytes and granulocytes upon
105 estrogen-withdrawal (G. G. Wang *et al.*, 2006), and show the physiologically high dynamics
106 of S100A8 and S100A9 mRNA and protein expression during differentiation. In order to

107 detect genes involved in the regulation of S100A8/A9 expression in an unbiased manner, we
108 used a mouse Genome-Scale CRISPR/Cas9 Knockout (GeCKO) library and screened for
109 monocytes with reduced or absent S100A9 expression. We thereby identified the
110 CCAAT/enhancer binding protein-family member C/EBP δ as a direct transcriptional regulator
111 of S100A8/A9. Furthermore, we found that the epigenetic factor JMJD3 contributes to
112 S100A8 and A9 expression in monocytes by erasure of the repressive histone mark
113 H3K27me₃ at *s100a8* and *a9* promoter regions. Moreover, we confirmed the clinical
114 relevance of this network in specific monocyte subpopulations in a cohort of patients with
115 cardiovascular disease.

116 RESULTS

117 *Genome-wide CRISPR/Cas9 Knockout screen reveals C/EBP δ as a regulatory factor of* 118 *S100A9 expression*

119 To detect genes involved in the regulation of S100A8/A9 expression, we established the
120 mouse GeCKO (Genome-Scale CRISPR-Cas9 Knockout) lentiviral pooled library designed in
121 Cas9 expressing ER-Hoxb8 cells. The used library contained a large mixture of CRISPR
122 sgRNA constructs, where six gRNAs per target gene increase efficiency and enable the
123 analysis of the molecular effects of many thousand genes in one experiment. After infection
124 of Cas9 expressing ER-Hoxb8 precursor cells with CRISPR library lentiviral particles, the
125 cells were differentiated for 3 days in the presence of GM-CSF to induce S100A8 and
126 S100A9 expression. Because we hypothesized that the parallel S100A8 and S100A9
127 expression is based on a common regulatory mechanism, we assumed that screening of one
128 of the two alarmins is sufficient in the first step. Therefore, cells with no or low S100A9
129 expression were selected by sorting and considered as hits, whereas the remaining cells
130 functioned as reference cells. To exclude phenotypes that are S100A9^{low/neg} due to
131 differentiation defects, we pre-gated for CD11b⁺Ly-6C⁺ monocytes. DNA of sorted cell pools
132 was purified and analysed by NGS (Figure 1, A). Intracellular S100A9-FITC staining of
133 precursor and differentiated Cas9 ER-Hoxb8 control monocytes was used as standard for

134 definition of sorting gates. Differentiated Cas9-library ER-Hoxb8 monocytes showed a wider
135 distribution among the gates, indicating the presence of S100A9^{low/neg} expressing cells due to
136 disruptions of regulatory genes caused by CRISPR/Cas9. A small amount of S100A9^{neg}
137 sorted cells were re-analysed by immunoblotting to validate S100A9 deficiency in this cell
138 population (Figure 1, B). Analysis of CRISPR KO library screen using the MAGeCK
139 method(Li *et al.*, 2014) resulted in a list of genes for which the respective gRNAs were
140 enriched in the hits sample. The highest number of gRNAs found within the top 20 hits
141 targeted *cebpd*, a gene encoding for a member of the CCAAT/Enhancer-Binding-protein
142 family, C/EBP δ (Figure 1, C).

143

144 *Decreased s100a8 and s100a9 expression in C/EBP δ KO monocytes*

145 We confirmed extraordinarily high dynamics of S100A8 and S100A9 expression during
146 monocyte/macrophage differentiation. ER-Hoxb8-derived monocytes show an about 590-fold
147 increase in *s100a8* mRNA expression and an about 1,800-fold increase of *s100a9* mRNA
148 expression on day 2 compared to day 0 of differentiation. At day 5 the *s100a8* mRNA
149 expression is already about 70-fold, the *s100a9* mRNA expression about 110-fold down-
150 regulated compared to day 2 of differentiation (Figure 2 A and B).

151 We confirmed the relevance of C/EBP δ for S100-expression by creating independent
152 C/EBP δ -deficient ER-Hoxb8 cells from C/EBP δ KO mice. Not only on differentiation day 3,
153 but already at the very beginning of differentiation, when *s100a8* and *a9* levels start to rise,
154 C/EBP δ -deficient ER-Hoxb8 monocytes showed significantly reduced levels of both, *s100a8*
155 (Figure 2, A) and *s100a9* mRNAs (Figure 2, B), compared to WT controls. The same effect
156 was detectable in C/EBP δ -deficient ER-Hoxb8 cells that were differentiated into the
157 neutrophilic lineage (Figure 2 – figure supplement 1, A). Accordingly, *cebpd* and *s100a8* and
158 *a9* mRNAs were co-expressed in differentiating WT monocytes and neutrophils, supporting a
159 mechanistic connection (Figure 2 – figure supplement 1, B and C). WT monocytes secret

160 significant S100A8/A9-protein amounts, whereas the supernatant of C/EBP δ KO monocytes
161 has up to 80% less S100A8/A9 (Figure 2, C). Consistent with this, serum S100A8/A9-levels
162 are significantly decreased in C/EBP δ KO mice (Figure 2, D). Although the proinflammatory
163 molecule S100A8/A9 is strongly reduced in the C/EBP δ KO monocytes, these cells exhibit
164 no general alterations of inflammatory functions, indicating a rather specific effect on
165 S100A8/A9-regulation than a general attenuation of inflammatory signaling due to C/EBP δ -
166 deficiency. Phagocytosis capacities are even elevated in C/EBP δ KO monocytes, very likely
167 through an already known PTX3-dependent mechanism (Ko *et al.*, 2012) (Figure 2 – figure
168 supplement 2, A and B), whereas ROS production is not influenced by C/EBP δ deficiency
169 (Figure 2 – figure supplement 2, C).

170 Interestingly, none of the transcription factors previously reported to target S100A8 and A9
171 were found within the hit list of our CRISPR KO library screen (Supplementary Table S1).
172 Nevertheless, to test the published candidate transcription factors ATF3, STAT3, KLF5, IRF7
173 and C/EBP β for their effects on S100A8 and A9-regulation, we created single KO ER-Hoxb8
174 cell lines of each individual candidate transcription factor. At no-time point during
175 differentiation, deficiency of the stated candidate transcription factors affected *s100a8* and
176 *s1009* expression, whereas C/EBP δ -deficiency has a strong attenuating effect on *s100a8*
177 and *s1009* expression, as shown on day 2 (Figure 2 – figure supplement 3, A and B).

178

179 *Enhanced C/EBP δ expression induces S100A8 and S100A9 expression*

180 To test the impact of C/EBP δ -induction on S100-alarmin expression, we infected C/EBP δ -
181 deficient ER-Hoxb8 cells with lentiviral particles carrying a tet-on system for doxycycline-
182 inducible 3xFlag-C/EBP δ expression (Figure 3, A). Doxycycline treatment led to expression
183 of the fusion protein 3xFlag-C/EBP δ , as revealed by western blot analysis (Figure 3, B) and
184 by qRT-PCR in comparison to C/EBP δ -deficient cells (Figure 3, C). Induction of 3xFlag-
185 C/EBP δ upon doxycycline-treatment led to increased *s100a8* and *s100a9* mRNA levels.
186 *Cebpd*, *s100a8* and *s100a9* mRNA levels in doxycycline-treated TRE_3xFlag-C/EBP δ cells

187 were comparable to WT cells at the same differentiation stage (Figure 3, D), demonstrating a
188 positive effect of C/EBP δ expression on S100A8/A9 regulation. Knockout of ATF3, a known
189 regulatory attenuator of *cebpd* expression (Litvak *et al.*, 2009), in ER-Hoxb8 monocytes led
190 to S100A8/A9 overexpression (Figure 2 – figure supplement 3), especially during early
191 stages of differentiation (Figure 3, E). ATF3 KO cells showed significantly elevated *cebpd*
192 level, indicating a C/EBP δ -mediated effect on the expression of *s100a8* and *a9* (Figure 3, F).
193 In the next step, we created FBXW7-deficient monocytes. FBXW7 is another well-known
194 attenuator of C/EBP δ expression (Balamurugan *et al.*, 2013). Lack of this antagonist resulted
195 in an even higher overexpression of *s100a8* and *s100a9* (Figure 3, G) with huge increases of
196 *cebpd* levels (Figure 3, H).

197 To confirm the biomedical relevance of the identified molecular network, we analysed the
198 expression of these genes in PBMCs and monocyte subpopulations of a subset of
199 participants in the BioNRW Study. Here, we found up-regulation of S100A8, S100A9 and
200 CEBPD in PBMCs of sCAD/MI cases, compared against controls (Figure 4, A), together with
201 a positive correlation of S100A8 and S100A9 expression with that of C/EBPD in these cells
202 (Figure 4, B and C). Moreover, there was also significant up-regulation of these three genes
203 specifically in classical monocytes, compared to intermediate and non-classical monocyte
204 subpopulations (Figure 4, D and E, for further comparisons see Supplementary Table S9). A
205 strong positive correlation between the expression of S100A8 and A9 and C/EBPD in these
206 monocyte subpopulations was found, suggesting that the expression of these genes is
207 mainly associated with the subset of pro-inflammatory monocytes. Interestingly, we also
208 found significant albeit milder, negative correlations between the expression of C/EBPD and
209 its antagonists FBXW7 and ATF3 in monocytes (Figure 4, F and G).

210

211 *C/EBP δ -binding sites within s100a8 and s100a9 promoter regions*

212 Chromatin immunoprecipitation revealed 3xFlag-C/EBP δ binding on *s100a8* and *s100a9*
213 promoter regions just before or within the predicted enhancers (Figure 5, A). Co-transfection

214 of HEK293T cells with GFP expressing S100-reporter vectors, together with doxycycline-
215 inducible 3xFlag-C/EBP δ vector (TRE_3xFlag-C/EBP δ) or its backbone lacking the 3xFlag-
216 C/EBP δ construct (TRE_ctrl), was performed to further examine specific C/EBP δ -binding
217 (Figure 5, B). Doxycycline-treatment resulted in 3xFlag-C/EBP δ protein expression after 24h
218 post-transfection in 3xFlag-C/EBP δ vector transfected cells (Figure 5, C). Transfection of
219 either *s100a8*-reporter construct (Figure 5, D) or *s100a9*-reporter construct (Figure 5, F)
220 together with 3xFlag-C/EBP δ vector led to enhanced GFP expression upon doxycycline-
221 treatment, in comparison to co-transfection with backbone plasmid (TRE_ctrl). Next, we
222 modified predicted C/EBP-binding sites on S100 promoters by mutagenesis of the
223 corresponding vectors. Again, co-transfection of mutated S100 reporter vectors and
224 doxycycline-dependent 3xFlag-C/EBP δ vector was performed to analyse the relevance of
225 specific C/EBP δ -binding sites. Two sites within the *s100a8* promoter region, stated as site 2
226 and site 3 (Figure 5, E), and one within the *s100a9* promoter region, stated as site 4 (Figure
227 5, G), caused a reduced or absent GFP expression upon co-transfection when deleted.
228 These binding sites, in turn, were located within the *s100a8* and *s100a9* promoter regions
229 where C/EBP δ -binding was confirmed by ChIP (Figure 5, A).

230

231 *Epigenetic landscape on s100 promoter regions reflects S100A8 and S100A9 expression in*
232 *monocytes*

233 Regulation of gene expression relies on variable factors; among these are chromatin
234 structure and epigenetic features. To measure changes in chromatin accessibility in
235 monocytic-progenitors and in S100A8/A9 expressing monocytes, we performed ATAC-seq of
236 precursor and differentiated ER-Hoxb8 cells. This revealed over 20,000 regions with
237 differential peaks (Figure 6, A). Openness of chromatin between precursor and differentiated
238 cells was highly different, as shown by principal component analysis (Figure 6, B). Among
239 the regions with significantly higher ATAC-seq reads in differentiated samples were the
240 *s100a8* and *s100a9* promoter and enhancer locations (Figure 6, C). Consistent with the

241 changes in chromatin accessibility at *s100* promoter regions during differentiation, we also
242 found changes in histone marks by ChIP. H3K27 acetylation (H3K27ac), a marker for active
243 transcription, was increased at differentiation day 3 in monocytes over precursor cells at
244 *s100a8* (Figure 6, D) and *s100a9* loci (Figure 6, E) in both, WT and C/EBP δ KO cells. In
245 contrast, tri-methylated H3K27 (H3K27me₃), associated with gene silencing, was
246 overrepresented in precursor cells over differentiated cells at the same loci in WT cells,
247 whereas H3K27me₃ marks did not decrease over the course of differentiation in C/EBP δ KO
248 cells. Accordingly, tri-methylated H3K27 was increased in C/EBP δ KO monocytes, compared
249 to the WT counterparts (Figure 6, F and G).

250

251 *The histone demethylase JMJD3 drives s100a8/a9 expression in dependency of C/EBP δ*

252 Decreased S100 expression in C/EBP δ -deficient day 3 monocytes is mirrored in the
253 epigenetic landscape by only slightly decreased H3K27ac level, but highly increased
254 H3K27me₃ level at *s100* promoter regions. Erasure of tri-methylation and di-methylation at
255 H3K27 is known to be catalyzed by the histone demethylase JMJD3 (JmjC Domain-
256 Containing Protein 3) (Xiang *et al.*, 2007). We found decreased expression of *jmjd3* in
257 differentiated C/EBP δ KO monocytes, compared to WT cells at the same stage (Figure 7, A).
258 Further, we used the potent JMJD3 inhibitor GSK-J4 (Kruidenier *et al.*, 2012) to block H3K27
259 demethylation in differentiating ER-Hobx8 cells, and discovered significantly decreased
260 *s100a8* and *s100a9* expression in GSK-J4 treated WT cells (Figure 7, B). These mRNA
261 quantities were comparable to untreated C/EBP δ -deficient monocytes, whereas the effects
262 on *s100a8/a9* expression in GSK-J4-treated C/EBP δ -deficient monocytes, compared to the
263 untreated counterparts, were negligible (Figure 7, B). These effects of GSK-J4 on *s100a8*
264 and *s100a9* expression are in line with increased H3K27me₃ marks in GSK-J4-treated WT
265 monocytes, compared to untreated WT cells on both, *s100a8* (Figure 7, C) and *s100a9*
266 (Figure 7, D) promoter regions.

267

268 DISCUSSION

269 The ER-Hoxb8 cell system serves as a substitute for murine primary cells of myeloid origin
270 that can be differentiated into phagocytes, such as monocytes and neutrophils. Using this
271 system allows comparison with *in vitro* differentiated primary cells (G. G. Wang *et al.*, 2006)
272 and, therefore, provides an experimental cell model for analysis of S100A8 and S100A9
273 expression. Although the alarmin is regarded as key factors in various inflammatory
274 conditions (Foell and Roth, 2004), cancer types (Cross *et al.*, 2005) and cardiovascular
275 diseases (Frangogiannis, 2019), little is known about their transcriptional regulation. The
276 serum concentrations of alarmins correlate with disease severity and activity and, hence,
277 they are reliable biomarkers for monitoring several inflammatory diseases (Foell *et al.*, 2004;
278 Ehrchen *et al.*, 2009). The expression levels of S100A8 and S100A9 differ extremely during
279 myeloid differentiation and the promoters of their genes represent probably one of the most
280 dynamic regulatory elements in the myeloid lineage. Whereas both proteins are completely
281 absent in myeloid precursor cells, they are highly expressed in monocytes and neutrophils,
282 which suggests that highly dynamic regulatory mechanisms drive S100A8 and S100A9
283 expression.

284 The CRISPR/Cas9-mediated KO screening approach based on a lentiviral pooled library has
285 been used so far to investigate various mechanisms, such as immunity-related pathways and
286 cancer-modulating events (Kweon and Kim, 2018). In this study, our unbiased genome-wide
287 screening approach allowed the identification of C/EBP δ as a factor involved in S100A9
288 regulation during murine monocyte differentiation. We further focused our investigations on
289 *cebpd* because this gene was in the top list of the robust rank aggregation (RRA) scores and
290 showed the highest numbers of guide RNAs with efficient effects on S100A9 expression in
291 our screening. This redundancy of independent parameters helped to distinguish true
292 positive from false positive hits. Furthermore, a robust phenotype-of-interest, such as a clear
293 S100A9 protein signal at day 3 of monocyte differentiation, allowed reliable negative
294 selection in Cas9-library monocytes. Selection of remaining cells served as a reference

295 control to distinguish true from false positives. The specificity of our selection procedure was
296 confirmed at the protein level by western blot analysis of sorted cell populations.
297 CRISPR/Cas9-based functional genomic screening has been shown to be highly specific,
298 thereby causing fewer cases of false positives in direct comparison with knockdown analysis
299 by RNA interference (Shalem *et al.*, 2014). We were now able to identify a novel regulator of
300 S100A8 and S100A9 using this unbiased method. By pre-gating on CD11b⁺Ly-6C⁺
301 monocytes we revealed C/EBP δ as a specific and differentiation-independent regulator of
302 S100A8 and S100A9, excluding pathways linked to general functions or development of
303 phagocytes.

304 We confirmed that the transcription factor C/EBP δ is a direct regulator of S100A8 and
305 S100A9 in murine monocytes in independent approaches. C/EBP δ and S100A8/A9 are co-
306 expressed in differentiating monocytes, and induction of C/EBP δ clearly showed that the
307 expression of S100A8 and S100A9 was up-regulated by the presence of C/EBP δ . This
308 evidence was further supported by increased S100A8/A9 levels caused by deletion of ATF3
309 and FBXW7, which are natural inhibitors of C/EBP δ .

310 The specificity of our approach was further confirmed by the fact that deficiency of several
311 transcription factors, such as STAT3, KLF5, IRF7 and C/EBP β , described as S100A8/A9
312 regulators in previous studies (Kuruto-Niwa *et al.*, 1998; Fujii, Manabe and Nagai, 2011; Lee
313 *et al.*, 2012; Liu *et al.*, 2016; Yang *et al.*, 2017), did not affect S100A8 and S100A9
314 expression in our ER-Hoxb8 monocytes.

315 Our ChIP data clearly showed that C/EBP δ specifically binds within *s100a8* and *s100a9*
316 promoter regions. Co-transfection of an inducible C/EBP δ -construct and *s100a8* and *s100a9*
317 reporter constructs not only demonstrated *s100* promoter activation due to C/EBP δ
318 expression, but also revealed functional relevance of specific binding sites, via promoter
319 bashing, that are located exactly within the stated promoter regions. The two DNA-motifs for
320 specific C/EBP δ responses on the *s100a8* promoter regions did not share the core sequence
321 5'-C/G GCAAT-3' that we found within the *s100a9* promoter region in our study. The latter

322 has been described in three other promoters, the human *pparg2* promoter (Lai *et al.*, 2008),
323 the murine and human *cebpd* promoter itself (Wang *et al.*, 2021) and the human *cox-2*
324 promoter (J. M. Wang *et al.*, 2006). We were able to show that the functionally relevant
325 C/EBP δ binding sites within the S100 promoters lie within genome regions which switch from
326 closed to open chromatin states during monocyte differentiation, and concomitant induction
327 of S100 expression as examined by ATAC-seq.

328 Our chromatin accessibility data on *s100a8* and *s100a9* promoter regions reflected active
329 *s100a8* and *s100a9* transcription and was supported by the characterization of the epigenetic
330 landscape using H3K27ac and H3K27me₃ marks. The fact that H3K27me₃ marks were
331 strongly decreased in WT monocytes, but not in precursors or C/EBP δ -deficient monocytes,
332 showed the indispensability of H3K27 demethylation for S100A8/A9 expression. Moreover,
333 our data demonstrated that the Jumonji C family histone demethylase JMJD3 regulates
334 S100A8/A9 expression by erasure of H3K27me₃ in dependency of C/EBP δ , which was
335 confirmed by GSK-J4-mediated inhibition of JMJD3 activities. Neither a link of C/EBP δ , nor
336 of S100A8/A9 and JMJD3 has been published yet. It has been shown that histone
337 demethylase activities of recombinant JMJD3 on mono-nucleosome substrates is relatively
338 low in contrast to higher activities on bulk histones (Lan *et al.*, 2007), suggesting that further
339 factors, such as C/EBP δ , are involved in chromatin binding. Several studies highlight JMJD3
340 as a regulator of innate immune responses, especially via NF- κ B-mediated inflammation in
341 macrophages (Na *et al.*, 2016, 2017; Davis *et al.*, 2020). Accordingly, knockdown of JMJD3
342 affected mainly inflammatory response networks in monocytic THP-1 cells (Das *et al.*, 2012)
343 and blocked activation of the NLRP3 inflammasome in bone marrow-derived macrophages
344 (Huang *et al.*, 2020). GSK-J4 treatment of mice attenuated disease progression and
345 inflammatory activities in several mouse models for inflammatory diseases, such as arthritis
346 (Jia *et al.*, 2018), colitis (Huang *et al.*, 2020) and EAE (experimental autoimmune
347 encephalomyelitis) (Doñas *et al.*, 2016). Accordingly, GSK-J4 treatment of our ER-Hoxb8
348 monocytes reduced expression of the proinflammatory alarmin S100A8/A9, which have been
349 shown to drive the inflammatory process of arthritis (Van Lent *et al.*, 2012). With our study,

350 we have taken a step forward to uncover the role of epigenetic features on S100A8 and
351 S100A9 expression and, thereby, on inflammatory conditions in murine monocytes.

352 We were also able to demonstrate an association of C/EBP δ and S100A8/A9 expression in
353 the context of human cardiovascular disease. We did not only show that expression of these
354 molecules show a significant positive correlation to each other but also to the manifestation
355 of stable coronary artery disease (sCAD) and myocardial infarction (MI) in patient derived
356 PBMCs. Moreover, expression of C/EBP δ and S100A8/A9 showed an even stronger
357 association with classical, proinflammatory monocytes (CD14⁺⁺CD16⁻), compared to non-
358 classical (CD14⁺CD16⁺⁺) and intermediate (CD14⁺⁺CD16⁺) monocytes. The endogenous
359 antagonists of C/EBP δ , ATF3 and especially FBXW7, showed a negative correlation of their
360 expression pattern in these monocyte subpopulations. Interestingly, inflammatory monocytes
361 with phagocytic and proteolytic activities have been reported to show an early peak at infarct
362 sites, which are followed by infiltration of non-classical, anti-inflammatory monocytes
363 (Nahrendorf *et al.*, 2007; Dutta and Nahrendorf, 2015). Genetic deletion of S100A8/A9 was
364 reported to attenuate MI and improve cardiac function in murine models. In contrast,
365 overexpression of S100A9 in mice increased infarct size and mortality, and treatment with
366 recombinant S100 proteins raised influx of immune cells into the infarct area (Li *et al.*, 2019;
367 Sreejit *et al.*, 2020). Moreover, serum concentrations of S100A8/A9 are known to be highly
368 sensitive and prognostic markers for myocardial injury (Aydin *et al.*, 2019). Taken together,
369 these data indicate that the C/EBP δ -S100-alarmin axis drives a clinically relevant
370 pathomechanism in cardiovascular disease and probably other inflammatory driven
371 conditions.

372 There are several published reports suggesting a biomedical relevance of the link between
373 the C/EBP δ and S100A8/A9 alarmin under other inflammatory conditions as well. For
374 example, C/EBP δ has been shown to play a role in the pathogenesis of psoriasis (Lan *et al.*,
375 2020) and in acute inflammatory signaling by regulating COX-2 (Wadleigh *et al.*, 2000), IL-6
376 (Litvak *et al.*, 2009) and TLR4 (Balamurugan *et al.*, 2013). Analysis of the genome-wide

377 transcription pattern of monocytes revealed IL-6 as the top gene induced by S100 alarmin
378 stimulation via interaction with TLR4 (Fassl *et al.*, 2015), and targeted deletion of S100A9
379 ameliorated inflammation in a murine psoriasis model(Zenz *et al.*, 2007). Additionally,
380 C/EBP δ levels were elevated in mouse models and patients of Alzheimer's disease (AD) (Li
381 *et al.*, 2004; Ko *et al.*, 2012) and rheumatoid arthritis (RA) (Nishioka *et al.*, 2000; Chang *et*
382 *al.*, 2012). In mouse models of AD, down-regulation (Ha *et al.*, 2010) and deficiency of
383 S100A9 (Kummer *et al.*, 2012) had therapeutic effects on disease activity. Also in human
384 studies, S100A9 was found to be associated with AD pathogenesis (Shepherd *et al.*, 2006).
385 Beyond that, S100A8 and S100A9 are known key players in the pathogenesis of arthritis in
386 murine models (Van Lent *et al.*, 2012). Gene expression profiling of blood cells from RA
387 patients receiving anti-TNF- α -based treatment showed that both C/EBP δ and S100A8 were
388 downregulated by the treatment (Meugnier *et al.*, 2011). Uncontrolled activity of S100A8/A9
389 alarmins drives TNF-induced arthritis in mice (Vogl *et al.*, 2018).

390 In the context of human RA, the expression and serum concentrations of S100A8/A9
391 correlate very well with disease activity and are the first predictive marker for disease
392 relapses in juvenile patients, and of the responses to therapy in juvenile and adult patients
393 (Moncrieffe *et al.*, 2013; Choi *et al.*, 2015). However, no direct molecular or functional link
394 between S100A8/A9 and C/EBP δ in arthritis has yet been reported.

395 MATERIAL & METHODS

396 Cell culture

397 ER-Hoxb8 cells were generated as described earlier (G. G. Wang *et al.*, 2006) and grown in
398 RPMI medium (Thermo Fisher Scientific) supplemented with 10% FBS (Biowest), 1%
399 penicillin/streptomycin solution (Sigma-Aldrich), 1% glutamine solution
400 (Thermo Fisher Scientific) 40 ng/ml rmGM-CSF (ImmunoTools) and 1 μ M β -estradiol (Sigma-
401 Aldrich). For differentiation, precursor cells were washed and incubated in estradiol-free
402 medium containing 40 ng/ml rmGM-CSF for several days. HEK293T were grown in DMEM
403 (Thermo Fisher Scientific) supplemented with 10% FBS (Biowest) and 1%
404 penicillin/streptomycin solution (Sigma-Aldrich), 1% glutamine solution (Thermo Fisher
405 Scientific), and 1% sodium pyruvate (Merck). All cell lines were cultured at 37 °C, 5% CO₂
406 and routinely screened and found negative for mycoplasma contamination in a PCR-based
407 assay (PromoCell).

408 Cell generation and manipulation

409 WT, C/EBP δ KO (kindly provided by Esta Sterneck, National Cancer Institute, Frederick, MD,
410 USA) (Sterneck *et al.*, 1998) and Cas9 expressing (Chiou *et al.*, 2015) cells originated from
411 corresponding mice. FBXW7, ATF3, STAT3, KLF5, IRF7 and C/EBP β KO ER-Hoxb8 cells
412 were generated using CRISPR/Cas9 as described earlier (Gran *et al.*, 2018). The oligos for
413 gRNA cloning are listed in Supplementary Table S2. For lentiviral production, the lentiGuide-
414 Puro (for GeCKO screen), lentiCRISPRv2-gRNA (for single KO cell lines) or TRE_3xFlag-
415 C/EBP δ was co-transfected into HEK293T cells, together with the packaging plasmids
416 pCMV-VSV-G (AddGene, #8454) and psPAX2 (AddGene, #12260). For transduction of ER-
417 Hoxb8 cells, cells were incubated with lentiviral particles and 8 μ g/ml polybrene (Sigma-
418 Aldrich) for 1 hour upon spinfection and selected for several days using puromycin
419 (InvivoGen). For transfection of HEK293T cells, the cells were seeded one day prior to
420 transfection. Then, cells were co-transfected with TRE_3xFlag-C/EBP δ and *s100a8* reporter

421 or *s100a9* reporter using the Lipofectamine™ 3000 Transfection Reagent (Thermo Scientific)
422 according to the manufacturer manual. For inhibition of JMJD3-activities, cells were treated
423 using 5 µM GSK-J4 HCl (SellekChem) for 3 days. To induce *cebpd* in TRE_3xFlag-C/EBPδ
424 ER-Hoxb8 cells or transfected HEK293T cells, cells were treated using 2 µg/mL doxycycline
425 (Sigma-Aldrich) for 24 hours.

426 **GeCKO-library screening**

427 Amplification of mouse CRISPR Knockout pooled library (GeCKO v2) in lentiGuide-Puro
428 plasmid, purchased from AddGene (#1000000053) (Sanjana, Shalem and Zhang, 2014),
429 was performed as described (Joung *et al.*, 2017). Cas9 expressing ER-Hoxb8 cells,
430 transduced with library lentiviral particles at a MOI of 0.4, were differentiated to day 3.
431 Intracellular S100A9 was stained with a S100A9-FITC coupled antibody using the
432 Foxp3/Transcription Factor Staining Buffer Set (eBioscience). Cells with no/lower S100A9
433 expression (hits) and cells with normal S100A9 expression (reference) were sorted using a
434 SH800S Cell Sorter (Sony, Minato, Japan) and DNA was purified by phenol-chloroform
435 extraction. Next generation sequencing was performed as described earlier (Joung *et al.*,
436 2017). Briefly, sgRNA library for next generation sequencing was prepared via PCR using
437 primers amplifying the target region with Illumina adapter sequences (Supplementary Table
438 S3), the purified DNA and the NEBNext® High-Fidelity 2X PCR Master Mix (NEB). PCR
439 reactions were pooled and purified using the QIAquick PCR Purification Kit (Qiagen). Size
440 and quantity was determined using the Bioanalyzer High Sensitivity DNA Analysis Agilent
441 High Sensitivity DNA Kit (Agilent). Samples were sequenced according to the Illumina user
442 manual with 80 cycles of read 1 (forward) using the NextSeq 500/550 High Output Kit v2.5
443 (75 Cycles) (Illumina) with the 20% PhiX spike in Illumina PhiX control kit (Illumina).

444 **Cloning and plasmid production**

445 *TRE_3xFlag-C/EBP δ and TRE_ctrl*

446 The pcDNA 3.1 (-) mouse C/EBP δ expression vector (AddGene, #12559) and annealed
447 oligonucleotides (Supplementary Table S4) were digested using *XbaI* and *EcoRI* and then
448 ligated. Using primers carrying restriction enzyme recognition sites (Supplementary
449 Table S4), the 3xFlag-C/EBP δ expression cassette was amplified. The resulting amplicon
450 and the pCW57.1 mDux-CA target vector (AddGene, #99284) (Whiddon *et al.*, 2017) were
451 digested using *NheI* and *AgeI* and subsequently ligated. TRE_ctrl was produced by digesting
452 TRE_3xFlag-C/EBP δ using *NheI* and *AgeI* and by subsequent blunting of ends by 3'
453 overhang removal and fill-in of 3' recessed (5' overhang) ends using DNA Polymerase I,
454 Large (Klenow) Fragment (NEB) prior to ligation.

455 *S100a8 and s100a9 reporter*

456 To construct *s100*-reporter vectors, 1500 bp upstream of *s100a8* and 1800 bp upstream of
457 *s100a9* transcription start sites were amplified from genomic mouse DNA. Using primers
458 carrying restriction enzyme recognition sites (Supplementary Table S5), promoter regions
459 were amplified and cloned into pLenti CMV GFP Blast vector (AddGene, #17445) (Campeau
460 *et al.*, 2009) using *XbaI* and *Clal*. Resulting *s100*prom-GFP constructs were cloned into
461 MSCV-PIG-empty vector (AddGene, #105594) (Xu *et al.*, 2018) by digestion with *NsiI* and
462 *Clal* together with the MSCV-backbone to exchange IRES-GFP-cassette with
463 *s100a8/a9*prom-GFP-cassette and subsequent ligation. Proposed C/EBP DNA binding sites
464 within *s100a8* and *s100a9* promoter regions were identified using the AliBaba2.1 net-based
465 transcription factor binding site (TFBS) search tool (Grabe, 2002), and were mutated by
466 deleting 6-7 base pairs using the QuikChange II XL Site-Directed Mutagenesis Kit (Agilent
467 Technologies). The primers used for mutagenesis are listed in Supplementary Table S6.
468 Plasmids were produced in DH5 α cells and purified using the PureLinkTM HiPure Plasmid
469 Midiprep Kit (ThermoScientific).

470 **Quantitative reverse transcription polymerase chain reaction (qRT-PCR)**

471 RNA was isolated using a NucleoSpin Extract II Isolation Kit (Macherey Nagel). The mRNA
472 expression of selected genes was measured by qRT-PCR as described earlier (Heming *et*
473 *al.*, 2018). The primers used are listed in Supplementary Table S7. The relative expression
474 level of each target gene was analysed using the $2^{-\Delta\Delta Cq}$ method and was normalised to
475 GAPDH.

476 **Chromatin immunoprecipitation (ChIP)**

477 For chromatin preparation, progenitor and differentiated ER-Hoxb8 cells were fixed using
478 1% formaldehyde for 5 minutes and reaction was stopped by adding 125 mM glycine.
479 Chromatin was extracted as previously described (Fujita and Fujii, 2013). Approximately 1-
480 5% of chromatin served as the input sample. DNA from input samples was isolated using
481 phenol-chloroform extraction as described earlier (Heming *et al.*, 2018). For
482 immunoprecipitation, 3 μ g antibody against Flag (Sigma-Aldrich, #F1804), H3K27ac (Abcam,
483 #ab4729), H3K27me₃ (Cell Signaling Technology, #9733), normal Rabbit IgG (Cell Signaling,
484 #2729) or Mouse IgG1, κ Isotype control (Biolegend, #400102) was conjugated to 900 μ g
485 magnetic Dynabeads-Protein G (Thermo Scientific, Waltham, MA) at 4 °C overnight.
486 Sonicated chromatin was added to AB-conjugated Dynabeads and incubated at 4 °C
487 overnight. The Dynabeads were washed as described earlier (Fujita and Fujii, 2013). For
488 elution, Dynabeads were incubated twice with elution buffer (0.05 M NaHCO₃, 1% SDS) at
489 65 °C for 15 minutes. DNA from eluates was isolated using phenol-chloroform extraction as
490 with input samples. Values were taken into account only when the amount of DNA pulled
491 down by using the antibody of interest was more than 5-fold increased over DNA pulled
492 down by using IgG antibodies. The primers used for ChIP-PCR are listed in Supplementary
493 Table S8.

494 **Assay for Transposase-Accessible Chromatin using sequencing (ATAC-seq)**

495 Precursor and day 3 differentiated WT ER-Hoxb8 cells were harvested, washed and
496 cryopreserved in 50% FBS/ 40% growth media/ 10% DMSO using a freezing container at -
497 80 °C overnight. Cells were shipped to Active Motif to perform ATAC-seq as previously
498 described (Buenrostro *et al.*, 2013).

499 **Measurements of S100A8/A9 protein level**

500 The S100A8/A9 protein concentrations were measured using an in-house S100A8/A9
501 enzyme-linked immunosorbent assay (ELISA), as previously described (Vogl *et al.*, 2014).

502 **Immunoblotting**

503 Cells were lysed in M-PER™ Mammalian Protein Extraction Reagent (Thermo Scientific,
504 Waltham) containing a protease inhibitor mixture (Sigma-Aldrich). Protein concentration was
505 determined, and equal amounts (15-30 µg) were run on a SDS-PAGE. After blotting on a
506 nitrocellulose membrane, the membrane was incubated overnight with primary antibodies
507 against: polyclonal rabbit S100A8 and S100A9 antibodies (originated from our own
508 production (Vogl *et al.*, 2014)), GAPDH (Cell Signaling Technology), α/β -Tubulin (Cell
509 Signaling Technology) and Flag (Sigma-Aldrich). Membranes were incubated with a HRP-
510 linked secondary antibody (Agilent, Santa Clara, CA) for 1 hour. Chemiluminescence signal
511 was detected using ChemiDoc XRS+ (Bio-Rad) together with ImageJ (National Institutes of
512 Health) to quantify the signal intensity.

513 **Phagocytosis of Latex Beads**

514 FluoSpheres polystyrene microspheres (ThermoScientific) were shortly sonicated in a bath
515 sonicator and added to cells at a ratio 1:10 for 2 h at 37 °C. The rate of phagocytosis was
516 determined by flow cytometry using Navios (Beckmann Coulter).

517 **Oxidative Burst**

518 Cells were stimulated using 10 nM PMA (Abcam) for 15 minutes or left untreated. After
519 incubation, 15 μ M DHR123 (Sigma-Aldrich) were added for another 15 min. The
520 fluorescence signal was analysed using flow cytometry (Navios, Beckmann Coulter).
521

522 **RNA-sequencing (RNA-seq)**

523 *Study population*

524 For this study, we used bulk mRNA-sequencing (RNA-seq) data of peripheral blood
525 mononuclear cells (PBMCs) and monocytes from two subsets of participants in the German
526 BioNRW Study. BioNRW actively recruits patients undergoing coronary angiography for the
527 diagnosis and percutaneous coronary intervention of coronary artery disease, as well as age
528 and gender matched healthy control individuals without history of cardiovascular disease, all
529 aged 18-70 years old. Patients receive standard cardiovascular care and medication (ACE-
530 inhibitor, AT1-receptor blocker, β -blocker, diuretics, statin), according to current guidelines.
531 Here, we included a total of 42 patients with stable coronary artery disease (sCAD) or acute
532 myocardial infarction (MI), as well as 39 of the corresponding age and sex matched controls.
533 The BioNRW Study is conducted in accordance with the guidelines of the Declaration of
534 Helsinki. The research protocol, including the case report forms, was approved by the local
535 ethics committee (#245-12). Written informed consent was obtained from all study
536 participants.

537 *Blood collection and isolation of PBMCs*

538 In case of MI, blood samples were collected during the first 4 days following the event. EDTA
539 blood was drawn from each subject by venipuncture. Sample processing followed within two
540 hours. PBMCs were obtained from 40 mL blood by density gradient centrifugation (Ficoll;
541 Biochrom). Lymphocytes were collected and washed twice with PBS. The pellet was re-
542 suspended in freezing medium Cryo-SFM (PromoCell) and cryopreserved.

543 *Isolation of monocyte subpopulations*

544 After washing, PBMCs were stained with anti-human antibodies specific for CD2 (PE, RPA-
545 2.10, T-cell marker), CD14 (APC, M5E2, monocyte subset differentiation), CD15 (PE, HIM1,
546 granulocyte marker), CD16 (PE-Cy7, 3G8, monocyte subset differentiation), CD19 (PE,
547 HIB19, B-cell marker), CD56 (PE, MY31, NK-cell marker), CD335 (PE, 9E2, NK-cell marker),
548 HLA-DR (FITC, TU36, antigen-presenting cells) (all from BD Biosciences), as reported by
549 Cros et al. (2010). Cells were acquired on a FACS LSR II flow cytometer (BD Biosciences)
550 and analysed using FlowJo software version 10 (Treestar Inc.). For sorting of monocyte
551 subsets, PBMCs were stained and sorted on a MoFlo Astrios cell sorter (Beckman Coulter).
552 Cells were sorted in 1 mL of Isol-RNA lysis reagent (5-Prime GmbH) and frozen at -80°C .
553 To avoid gender-specific effects, 3 representative male samples of each BioNRW diagnostic
554 group (sCAD, MI and control) were selected to be subjected to cell sorting and subsequent
555 RNA isolation.

556

557 *Differential expression analysis in PBMCs and monocytes*

558 For mRNA profiling of PBMCs and monocyte subpopulations using RNA-Seq, mRNA was
559 enriched using the NEBNext® Poly(A) Magnetic Isolation Module (NEB), followed by cDNA
560 NGS library preparation (NEBNext® Ultra RNA Library Prep Kit for Illumina, NEB). The size
561 of the resulting libraries was controlled by the use of a Bioanalyzer High Sensitivity DNA Kit
562 (Agilent Technologies) and quantified using the KAPA Library Quantification Kit for Illumina
563 (Roche). Equimolar, appropriately pooled libraries were sequenced in a single read mode (75
564 cycles) on a NextSeq500 System (Illumina) using v2 chemistry, yielding in an average
565 QScore distribution of $92\% \geq Q30$ score. They were subsequently demultiplexed and
566 converted to FASTQ files using bcl2fastq v2.20 Conversion software (Illumina). Data was
567 quality controlled using FASTQC software and trimmed for adapter sequences using
568 Trimmomatic (Bolger, Lohse and Usadel, 2014).

569 **General statistics**

570 The statistical significance of the data was determined using Prism 5.0 software (GraphPad
571 Software, CA, USA). Analyses between two groups were performed using an unpaired two-
572 tailed Student's t-test. Comparisons among three or more groups were performed by using
573 one-way ANOVA, followed by Bonferroni's multiple means tests for comparing all pairs of
574 columns. Differences were considered statistically significant at a probability (p-value) of
575 <0.05.

576

577 **Bioinformatics analysis**

578 *GeCKO-library screening*

579 Analysis of counting the reads for each gRNA and differential analysis was performed using
580 Model-based Analysis of Genome-wide CRISPR-Cas9 Knockout (MaGeCK) 0.5.9.3, a
581 computational tool to identify important genes from GeCKO-based screens (Li *et al.*, 2014). A
582 modified RRA (Robust Rank Aggregation) method with a redefined ρ value was used.
583 Former RRA computed a significant P-value for genes in the middle of gRNA ranked list and
584 thereby introducing false positives because the assumption of uniformity is not necessarily
585 satisfied in real applications. Thus, top ranked % gRNAs were selected if their negative
586 binomial P-values were smaller than a threshold, such as 0.05. If j of the n gRNAs targeting a
587 gene were selected, then the modified value is defined as $\rho = \min(p_1, p_2, \dots, p_j)$, where $j \leq n$.
588 This modified RRA method could efficiently remove the effect of insignificant gRNAs in the
589 assessment of gene significance. A permutation test where the gRNAs were randomly
590 assigned to genes was performed to compute a P-value based on the ρ values. By default,
591 100 x n g permutations are performed, where n g is the number of genes. We then compute
592 the FDR from the empirical permutation P-values using the Benjamini-Hochberg procedure.

593 *ATAC-seq*

594 Sequence analysis was performed by mapping the paired-end 42 bp sequencing reads
595 (PE42) generated by Illumina sequencing (using NextSeq 500) to the genome using the
596 BWA algorithm with default settings (“bwa mem”). Only reads that passed Illumina’s purity
597 filter, aligned with no more than 2 mismatches, and mapped uniquely to the genome were
598 used in the subsequent analysis. In addition, duplicate reads (“PCR duplicates”) were
599 removed. For Peak finding, genomic regions with high levels of transposition/tagging events
600 were determined using the MACS2 peak calling algorithm (Zhang *et al.*, 2008). Both reads
601 (tags) from paired-end sequencing represent transposition events, both reads were used for
602 peak-calling but treated a single, independent reads. Fragment density was determined by
603 dividing the genome into 32 bp bins and by defining number of fragments in each bin. For
604 this purpose, reads were extended to 200 bp, which was close to the average length of the
605 sequenced library inserts. Differential regions were determined with the DESeq2
606 bioconductor package (Love, Huber and Anders, 2014) with absolute $\log_2FC > 0.3$ and an
607 FDR corrected $p < 0.1$.

608 *RNA seq*

609 The resulting reads were mapped to the human reference genome builds hg19 (monocytes)
610 or hg38 (PBMCs) using Tophat2 (Kim *et al.*, 2013) or HISAT2 v2.1.0 (Kim *et al.*, 2019),
611 counted by using the R package GenomicAlignments (Lawrence *et al.*, 2013) or HTSeq
612 v0.11.2 (Anders, Pyl and Huber, 2015), and followed by differential expression analysis using
613 DESeq2 (Love, Huber and Anders, 2014). The PBMCs dataset used for analysis consisted of
614 72 individuals, from which 36 were sCAD/MI cases and 36 were controls (21 females and 15
615 males in each group, mean age: 50.8 ± 12.3 years), while the monocytes dataset contained
616 read counts of classical, intermediate and non-classical monocyte subpopulations from 9
617 male individuals (3 MI, 3 sCAD and 3 controls. One sCAD non-classical monocyte sample
618 had to be excluded from analysis due to low mapping rate; therefore, the monocytes dataset
619 used for analysis contained 26 samples. Genes were considered differentially expressed at

620 adjusted $p < 0.05$ (Benjamini-Hochberg method). R was used to perform Pearson correlation
621 tests and generate plots for the genes of interest from the normalised count data.

622

623 **CONCLUSION**

624 We found that the transcription factor C/EBP δ drives expression of the abundant alarmins
625 S100A8 and S100A9, and demonstrated that C/EBP δ binding to specific sites on *s100a8* and
626 *s100a9* promoter regions also induced changes in chromatin accessibility via JMJD3-
627 mediated demethylation of H3K27me $_3$ marks, which includes a so far unknown link. Due to
628 the high relevance of S100A8/A9 alarmin expression in many inflammatory diseases, our
629 findings may point to novel molecular targets for innovative anti-inflammatory therapeutic
630 approaches.

631

632 **AUTHORSHIP**

633 Contribution: S.-L.J.-S., A.I.C., M.S., J.R., and O.F. conceived and designed the
634 experiments; S.-L.J.-S., A.W., J.W. and O.F. performed experiments; B.M. and B.S. recruited
635 the patients and provided the PBMCs and monocyte subsets from the Bio.NRW study; S.-
636 L.J.-S., M.H.-R., L.M., A.W., M.S., T.V., J.R. and O.F. analysed the data; and S.-L.J.-S., J.
637 R., and O.F. wrote the manuscript.

638

639 **ACKNOWLEDGEMENTS**

640 The authors thank Ursula Nordhues, Heike Berheide, Eva Nattkemper, Heike Harter, Elvira
641 Barg and Marianne Jansen-Rust for their excellent technical support, and Esta Sterneck
642 (Center for Cancer Research, National Cancer Institute, Frederick, MD) for providing the
643 C/EBP δ KO mice.

644 This work was supported by grants the Interdisciplinary Center of Clinical Research at the
645 University of Münster (Ro2/023/19, Vo2/011/19), the German Research Foundation CRC
646 1009 B8, B9 and Z2, CRU 342 P3 and P5 and RO 1190/14-1 (to J. Roth and T. Vogl) and by
647 the EU EFRE Bio.NRW programme (005-1007-0006) to M.S. The funders had no role in the
648 study design, data collection and analysis, decision to publish, or preparation of the
649 manuscript.

650

651 **DECLARATION OF INTEREST**

652 The authors declare no competing interests.

653 **RESOURCE AVAILABILTY**

654 **lead contact**

655 Further information and requests for resources and reagents should be directed to and will
656 be fulfilled by the lead contact, Johannes Roth (rothj@uni-muenster.de)

657

658 **materials availability**

659 Any resource and reagent in this paper is available from the lead contact upon request.

660

661 **data and code availability**

662 Human RNA-seq data have been deposited at the NCBI's BioProject Database with the ID
663 706411.

664

665 Jauch-Speer SL, Wolf J, Herrera-Rivero M, Martens L, Imam Chasan A, Witten A, Markus B,
666 Schieffer B, Vogl T, Stoll M, Roth J and Fehler O (2021) **GeCKO screen** ID PRJNA754262
667 at the NCBI's Database: [https://dataview.ncbi.nlm.nih.gov/object/PRJNA754262?reviewer=61](https://dataview.ncbi.nlm.nih.gov/object/PRJNA754262?reviewer=611pv4hrh8mcbvcne6psjulv)
668 [1pv4hrh8mcbvcne6psjulv](https://dataview.ncbi.nlm.nih.gov/object/PRJNA754262?reviewer=611pv4hrh8mcbvcne6psjulv)

669 Jauch-Speer SL, Wolf J, Herrera-Rivero M, Martens L, Imam Chasan A, Witten A, Markus B,
670 Schieffer B, Vogl T, Stoll M, Roth J and Fehler O (2021) **ATAC-seq in precursor and**
671 **differentiated ER-Hoxb8 cells** ID PRJNA755208 at the NCBI's Database:
672 <https://dataview.ncbi.nlm.nih.gov/object/PRJNA755208?reviewer=ivcq37bj1esdf9n7vl6l83m3>
673 [ed](#)

674 **REFERNCES**

- 675 Anders, S., Pyl, P. T. and Huber, W. (2015) 'HTSeq--a Python framework to work with high-
- 676 throughput sequencing data.', *Bioinformatics (Oxford, England)*, 31(2), pp. 166–169. doi:
- 677 10.1093/bioinformatics/btu638.
- 678 Austermann, J., Spiekermann, C. and Roth, J. (2018) 'S100 proteins in rheumatic diseases',
- 679 *Nature Reviews Rheumatology*. Springer US, 14(9), pp. 528–541. doi: 10.1038/s41584-018-
- 680 0058-9.
- 681 Aydin, Suleyman *et al.* (2019) 'Biomarkers in acute myocardial infarction: current
- 682 perspectives.', *Vascular health and risk management*, 15, pp. 1–10. doi:
- 683 10.2147/VHRM.S166157.
- 684 Balamurugan, K. *et al.* (2013) 'FBXW7 α attenuates inflammatory signalling by
- 685 downregulating C/EBP δ and its target gene Tlr4', *Nature communications*, 4(1662). doi:
- 686 10.1038/ncomms2677.FBXW7.
- 687 Bolger, A. M., Lohse, M. and Usadel, B. (2014) 'Trimmomatic: a flexible trimmer for Illumina
- 688 sequence data.', *Bioinformatics (Oxford, England)*, 30(15), pp. 2114–2120. doi:
- 689 10.1093/bioinformatics/btu170.
- 690 Buenrostro, J. D. *et al.* (2013) 'Transposition of native chromatin for fast and sensitive
- 691 epigenomic profiling of open chromatin, DNA-binding proteins and nucleosome position',
- 692 *Nature Methods*, 10(12), pp. 1213–1218. doi: 10.1038/nmeth.2688.
- 693 Campeau, E. *et al.* (2009) 'A versatile viral system for expression and depletion of proteins in
- 694 mammalian cells', *PLoS ONE*, 4(8). doi: 10.1371/journal.pone.0006529.
- 695 Chang, L. H. *et al.* (2012) 'Role of Macrophage CCAAT/Enhancer Binding Protein Delta in
- 696 the Pathogenesis of Rheumatoid Arthritis in Collagen-Induced Arthritic Mice', *PLoS ONE*,
- 697 7(9). doi: 10.1371/journal.pone.0045378.
- 698 Chiou, S. *et al.* (2015) 'Pancreatic cancer modeling using retrograde viral vector delivery and

- 699 in vivo CRISPR/Cas9-mediated somatic genome editing', *Genes and Development*, pp.
700 1576–1585. doi: 10.1101/gad.264861.115.1576.
- 701 Choi, I. Y. *et al.* (2015) 'MRP8/14 serum levels as a strong predictor of response to biological
702 treatments in patients with rheumatoid arthritis', *Annals of the Rheumatic Diseases*, 74(3),
703 pp. 499–505. doi: 10.1136/annrheumdis-2013-203923.
- 704 Cros, J. *et al.* (2010) 'Human CD14dim monocytes patrol and sense nucleic acids and
705 viruses via TLR7 and TLR8 receptors.', *Immunity*, 33(3), pp. 375–386. doi:
706 10.1016/j.immuni.2010.08.012.
- 707 Cross, S. S. *et al.* (2005) 'Expression of S100 proteins in normal human tissues and common
708 cancers using tissue microarrays: S100A6, S100A8, S100A9 and S100A11 are all
709 overexpressed in common cancers', *Histopathology*, 46(3), pp. 256–269. doi:
710 10.1111/j.1365-2559.2005.02097.x.
- 711 Das, N. D. *et al.* (2012) 'Gene networking and inflammatory pathway analysis in a JMJD3
712 knockdown human monocytic cell line', *Cell Biochemistry and Function*, 30(3), pp. 224–232.
713 doi: 10.1002/cbf.1839.
- 714 Davis, F. M. *et al.* (2020) 'Palmitate-TLR4 signaling regulates the histone demethylase,
715 JMJD3, in macrophages and impairs diabetic wound healing', *European Journal of*
716 *Immunology*, 50(12), pp. 1929–1940. doi: 10.1002/eji.202048651.
- 717 Doñas, C. *et al.* (2016) 'The histone demethylase inhibitor GSK-J4 limits inflammation
718 through the induction of a tolerogenic phenotype on DCs', *Journal of Autoimmunity*, 75, pp.
719 105–117. doi: 10.1016/j.jaut.2016.07.011.
- 720 Dutta, P. and Nahrendorf, M. (2015) 'Monocytes in Myocardial Infarction', *Arteriosclerosis,*
721 *Thrombosis, and Vascular Biology*, 35(5), pp. 1066–1070. doi:
722 10.1161/ATVBAHA.114.304652.
- 723 Ehrchen, J. M. *et al.* (2009) 'The endogenous Toll-like receptor 4 agonist S100A8/S100A9

- 724 (calprotectin) as innate amplifier of infection, autoimmunity, and cancer.’, *Journal of*
725 *leukocyte biology*, 86(3), pp. 557–566. doi: 10.1189/jlb.1008647.
- 726 Fassl, S. K. *et al.* (2015) ‘Transcriptome Assessment Reveals a Dominant Role for TLR4 in
727 the Activation of Human Monocytes by the Alarmin MRP8’, *The Journal of Immunology*,
728 194(2), pp. 575–583. doi: 10.4049/jimmunol.1401085.
- 729 Foell, D. *et al.* (2004) ‘Phagocyte-specific calcium-binding S100 proteins as clinical
730 laboratory markers of inflammation’, *Clinica Chimica Acta*, 344(1–2), pp. 37–51. doi:
731 10.1016/j.cccn.2004.02.023.
- 732 Foell, D. and Roth, J. (2004) ‘Proinflammatory S100 proteins in arthritis and autoimmune
733 disease’, *Arthritis and Rheumatism*, 50(12), pp. 3762–3771. doi: 10.1002/art.20631.
- 734 Frangogiannis, N. G. (2019) ‘S100A8/A9 as a therapeutic target in myocardial infarction:
735 cellular mechanisms, molecular interactions, and translational challenges’, *European Heart*
736 *Journal*, 40(32), pp. 2724–2726. doi: 10.1093/eurheartj/ehz524.
- 737 Freise, N. *et al.* (2019) ‘Signaling mechanisms inducing hyporesponsiveness of phagocytes
738 during systemic inflammation’, *Blood*, 134(2), pp. 134–146. doi: 10.1182/blood.2019000320.
- 739 Fujita, T. and Fujii, H. (2013) ‘Efficient isolation of specific genomic regions and identification
740 of associated proteins by engineered DNA-binding molecule-mediated chromatin
741 immunoprecipitation (enChIP) using CRISPR’, *Biochemical and Biophysical Research*
742 *Communications*. Elsevier Inc., 439(1), pp. 132–136. doi: 10.1016/j.bbrc.2013.08.013.
- 743 Fujii, K., Manabe, I. and Nagai, R. (2011) ‘Renal collecting duct epithelial cells regulate
744 inflammation in tubulointerstitial damage in mice’, *The Journal of Clinical Investigation*, 121(9),
745 pp. 3425–3441. doi: 10.1172/JCI57582.the.
- 746 Grabe, N. (2002) ‘AliBaba2: Context Specific Identification of Transcription Factor Binding
747 Sites’, *In Silico Biology*. IOS Press, 2, pp. S1–S15.

- 748 Gran, S. *et al.* (2018) 'Imaging, myeloid precursor immortalization, and genome editing for
749 defining mechanisms of leukocyte recruitment in vivo', *Theranostics*, 8(9), pp. 2407–2423.
750 doi: 10.7150/thno.23632.
- 751 Ha, T. Y. *et al.* (2010) 'S100a9 knockdown decreases the memory impairment and the
752 neuropathology in Tg2576 mice, AD animal model', *PLoS ONE*, 5(1). doi:
753 10.1371/journal.pone.0008840.
- 754 Heming, M. *et al.* (2018) 'Peroxisome proliferator-activated receptor- γ modulates the
755 response of macrophages to lipopolysaccharide and glucocorticoids', *Frontiers in*
756 *Immunology*, 9(MAY). doi: 10.3389/fimmu.2018.00893.
- 757 Hessian, P. A., Edgeworth, J. and Hogg, N. (1993) 'MRP-8 and MRP-14, two abundant
758 Ca(2+)-binding proteins of neutrophils and monocytes.', *J Leukoc Biol*, 53(February), pp.
759 197–204.
- 760 Huang, M. *et al.* (2020) 'Jmjd3 regulates inflammasome activation and aggravates DSS-
761 induced colitis in mice', *FASEB Journal*, 34(3), pp. 4107–4119. doi:
762 10.1096/fj.201902200RR.
- 763 Jia, W. *et al.* (2018) 'Histone demethylase JMJD3 regulates fibroblast-like synoviocyte-
764 mediated proliferation and joint destruction in rheumatoid arthritis', *FASEB Journal*, 32(7), pp.
765 4031–4042. doi: 10.1096/fj.201701483R.
- 766 Joung, J. *et al.* (2017) 'Genome-scale CRISPR-Cas9 knockout and transcriptional activation
767 screening', *Nature Protocols*. Nature Publishing Group, 12(4), pp. 828–863. doi:
768 10.1038/nprot.2017.016.
- 769 Kehl-Fie, T. E. *et al.* (2011) 'Nutrient Metal Sequestration by Calprotectin Inhibits Bacterial
770 Superoxide Defense, Enhancing Neutrophil Killing of Staphylococcus aureus', *Cell Host &*
771 *Microbe*, 10(2), pp. 158–164. doi: <https://doi.org/10.1016/j.chom.2011.07.004>.
- 772 Kehl-Fie, T. E. and Skaar, E. P. (2010) 'Nutritional immunity beyond iron: a role for

- 773 manganese and zinc', *Current Opinion in Chemical Biology*, 14(2), pp. 218–224. doi:
774 <https://doi.org/10.1016/j.cbpa.2009.11.008>.
- 775 Kim, D. *et al.* (2013) 'TopHat2: accurate alignment of transcriptomes in the presence of
776 insertions, deletions and gene fusions', *Genome Biology*, 14(4), p. R36. doi: 10.1186/gb-
777 2013-14-4-r36.
- 778 Kim, D. *et al.* (2019) 'Graph-based genome alignment and genotyping with HISAT2 and
779 HISAT-genotype.', *Nature biotechnology*, 37(8), pp. 907–915. doi: 10.1038/s41587-019-
780 0201-4.
- 781 Ko, C. Y. *et al.* (2012) 'CCAAT/enhancer binding protein delta (CEBPD) elevating PTX3
782 expression inhibits macrophage-mediated phagocytosis of dying neuron cells', *Neurobiology*
783 *of Aging*, 33(2), pp. 422.e11–422.e25. doi: 10.1016/j.neurobiolaging.2010.09.017.
- 784 Kruidenier, L. *et al.* (2012) 'A selective jumonji H3K27 demethylase inhibitor modulates the
785 proinflammatory macrophage response', *Nature*. Nature Publishing Group, 488(7411), pp.
786 404–408. doi: 10.1038/nature11262.
- 787 Kummer, M. P. *et al.* (2012) 'Mrp14 deficiency ameliorates amyloid β burden by increasing
788 microglial phagocytosis and modulation of amyloid precursor protein processing', *Journal of*
789 *Neuroscience*, 32(49), pp. 17824–17829. doi: 10.1523/JNEUROSCI.1504-12.2012.
- 790 Kuruto-Niwa, R. *et al.* (1998) 'Transcriptional regulation by C/EBP alpha and -beta in the
791 expression of the gene for the MRP14 myeloid calcium binding protein.', *Cell structure and*
792 *function*, 23(3), pp. 109–118.
- 793 Kweon, J. and Kim, Y. (2018) 'High-throughput genetic screens using CRISPR–Cas9
794 system', *Archives of Pharmacal Research*, 41(9), pp. 875–884. doi: 10.1007/s12272-018-
795 1029-z.
- 796 Lai, P. H. *et al.* (2008) 'HDAC1/HDAC3 modulates PPARG2 transcription through the
797 sumoylated CEBPD in hepatic lipogenesis', *Biochimica et Biophysica Acta - Molecular Cell*

- 798 *Research*, 1783(10), pp. 1803–1814. doi: 10.1016/j.bbamcr.2008.06.008.
- 799 Lan, F. *et al.* (2007) 'A histone H3 lysine 27 demethylase regulates animal posterior
800 development', *Nature*, 449(7163), pp. 689–694. doi: 10.1038/nature06192.
- 801 Lan, X. O. *et al.* (2020) 'Shikonin inhibits CEBPD downregulation in IL-17-treated HaCaT
802 cells and in an imiquimod-induced psoriasis model', *Molecular Medicine Reports*, 22(3), pp.
803 2263–2272. doi: 10.3892/mmr.2020.11315.
- 804 Lawrence, M. *et al.* (2013) 'Software for Computing and Annotating Genomic Ranges', *PLoS*
805 *Computational Biology*, 9(8), pp. 1–10. doi: 10.1371/journal.pcbi.1003118.
- 806 Lee, M. J. *et al.* (2012) 'Interleukin-6 Induces S100A9 Expression in Colonic Epithelial Cells
807 through STAT3 Activation in Experimental Ulcerative Colitis', *PLoS ONE*, 7(9). doi:
808 10.1371/journal.pone.0038801.
- 809 Van Lent, P. L. E. M. *et al.* (2008) 'Myeloid-related proteins S100A8/S100A9 regulate joint
810 inflammation and cartilage destruction during antigen-induced arthritis', *Annals of the*
811 *Rheumatic Diseases*, 67(12), pp. 1750–1758. doi: 10.1136/ard.2007.077800.
- 812 Van Lent, P. L. E. M. *et al.* (2012) 'Active involvement of alarmins S100A8 and S100A9 in the
813 regulation of synovial activation and joint destruction during mouse and human
814 osteoarthritis', *Arthritis and Rheumatism*, 64(5), pp. 1466–1476. doi: 10.1002/art.34315.
- 815 Leukert, N. *et al.* (2006) 'Calcium-dependent Tetramer Formation of S100A8 and S100A9 is
816 Essential for Biological Activity', *Journal of Molecular Biology*, 359(4), pp. 961–972. doi:
817 10.1016/j.jmb.2006.04.009.
- 818 Li, R. *et al.* (2004) 'CCAAT/enhancer binding protein δ (C/EBP δ) expression and elevation in
819 Alzheimer's disease', *Neurobiology of Aging*, 25(8), pp. 991–999. doi:
820 10.1016/j.neurobiolaging.2003.10.016.
- 821 Li, W. *et al.* (2014) 'MAGeCK enables robust identification of essential genes from genome-

- 822 scale CRISPR/Cas9 knockout screens', *Genome Biology*, 15(12), p. 554. doi:
823 10.1186/preaccept-1316450832143458.
- 824 Li, Y. *et al.* (2019) 'S100a8/a9 Signaling Causes Mitochondrial Dysfunction and
825 Cardiomyocyte Death in Response to Ischemic/Reperfusion Injury', *Circulation*, 140(9), pp.
826 751–764. doi: 10.1161/CIRCULATIONAHA.118.039262.
- 827 Litvak, V. *et al.* (2009) 'Function of C/EBP δ in a regulatory circuit that discriminates between
828 transient and persistent TLR4-induced signals', *Nature Immunology*, 10(4), pp. 437–443. doi:
829 10.1038/ni.1721.
- 830 Liu, Y. F. *et al.* (2016) 'Glucocorticoid induces hepatic steatosis by inhibiting activating
831 transcription factor 3 (ATF3)/S100A9 protein signaling in granulocytic myeloid-derived
832 suppressor cells', *Journal of Biological Chemistry*, 291(41), pp. 21771–21785. doi:
833 10.1074/jbc.M116.726364.
- 834 Loser, K. *et al.* (2010) 'The toll-like receptor 4 ligands Mrp8 and Mrp14 are crucial in the
835 development of autoreactive CD8+ T cells', *Nature Medicine*. Nature Publishing Group,
836 16(6), pp. 713–717. doi: 10.1038/nm.2150.
- 837 Love, M. I., Huber, W. and Anders, S. (2014) 'Moderated estimation of fold change and
838 dispersion for RNA-seq data with DESeq2', *Genome Biology*, 15(12), p. 550. doi:
839 10.1186/s13059-014-0550-8.
- 840 Meugnier, E. *et al.* (2011) 'Gene expression profiling in peripheral blood cells of patients with
841 rheumatoid arthritis in response to anti-TNF- α treatments', *Physiological Genomics*, 43(7),
842 pp. 365–371. doi: 10.1152/physiolgenomics.00127.2010.
- 843 Moncrieffe, H. *et al.* (2013) 'A subgroup of juvenile idiopathic arthritis patients who respond
844 well to methotrexate are identified by the serum biomarker MRP8/14 protein', *Rheumatology*,
845 52(8), pp. 1467–1476. doi: 10.1093/rheumatology/ket152.
- 846 Na, J. *et al.* (2016) 'Histone H3K27 Demethylase JMJD3 in Cooperation with NF- κ B

847 Regulates Keratinocyte Wound Healing', *Journal of Investigative Dermatology*. The Authors,
848 136(4), pp. 847–858. doi: 10.1016/j.jid.2015.11.029.

849 Na, J. *et al.* (2017) 'JMJD3 and NF- κ B-dependent activation of Notch1 gene is required for
850 keratinocyte migration during skin wound healing', *Scientific Reports*. Springer US, 7(1), pp.
851 1–12. doi: 10.1038/s41598-017-06750-7.

852 Nahrendorf, M. *et al.* (2007) 'The healing myocardium sequentially mobilizes two monocyte
853 subsets with divergent and complementary functions', *The Journal of experimental medicine*.
854 2007/11/19. The Rockefeller University Press, 204(12), pp. 3037–3047. doi:
855 10.1084/jem.20070885.

856 Nishioka, K. *et al.* (2000) 'Enhanced expression and DNA binding activity of two
857 CCAAT/enhancer-binding protein isoforms, C/EBP β and C/EBP δ , in rheumatoid synovium',
858 *Arthritis and Rheumatism*, 43(7), pp. 1591–1596. doi: 10.1002/1529-
859 0131(200007)43:7<1591::AID-ANR24>3.0.CO;2-9.

860 Sanjana, N. E., Shalem, O. and Zhang, F. (2014) 'Improved vectors and genome-wide
861 libraries for CRISPR screening', *Nature methods*, 11(8), pp. 783–784. doi:
862 10.1038/nmeth.3047.Improved.

863 Shalem, O. *et al.* (2014) 'Genome-Scale CRISPR-Cas9 Knockout Screening in Human
864 Cells', *Science*, 343(6166), pp. 84–87. doi: 10.1126/science.1247005.Genome-Scale.

865 Shepherd, C. E. *et al.* (2006) 'Inflammatory S100A9 and S100A12 proteins in Alzheimer's
866 disease', *Neurobiology of Aging*, 27(11), pp. 1554–1563. doi:
867 <https://doi.org/10.1016/j.neurobiolaging.2005.09.033>.

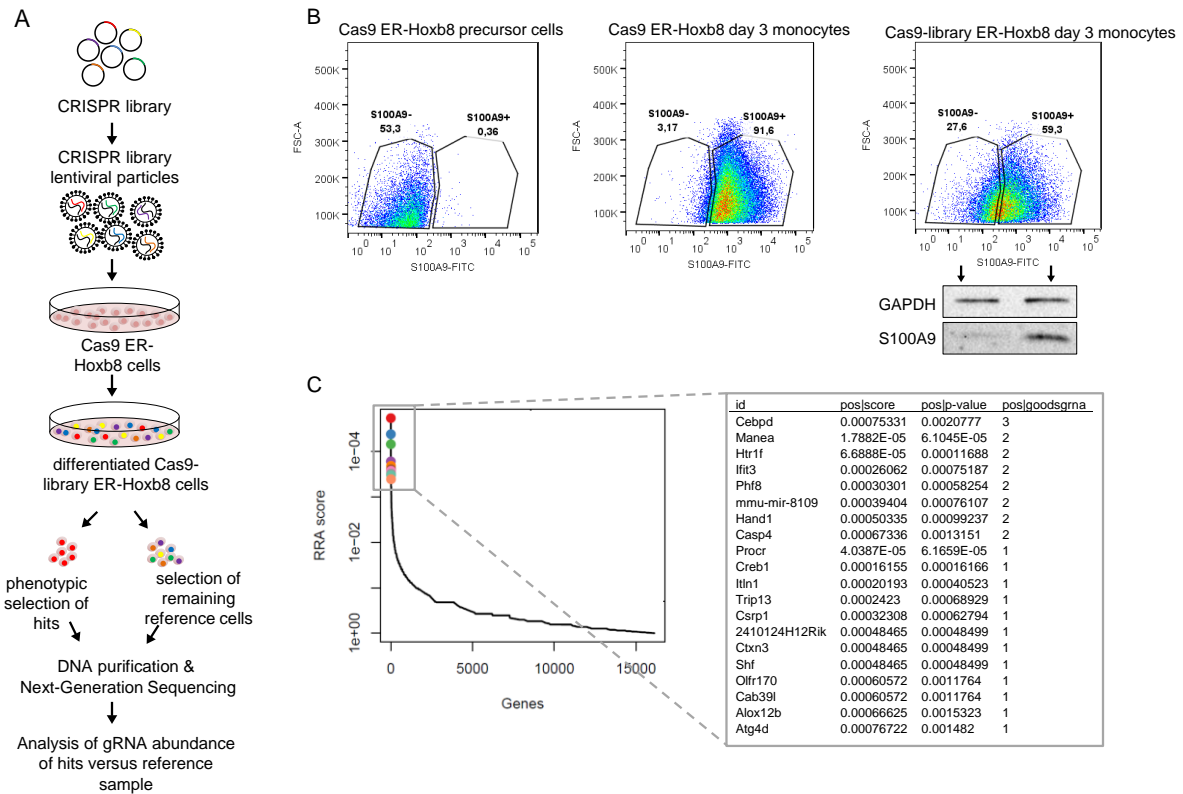
868 Sreejit, G. *et al.* (2020) 'Neutrophil-Derived S100A8/A9 Amplify Granulopoiesis After
869 Myocardial Infarction.', *Circulation*, 141(13), pp. 1080–1094. doi:
870 10.1161/CIRCULATIONAHA.119.043833.

871 Sterneck, E. *et al.* (1998) 'Selectively enhanced contextual fear conditioning in mice lacking

- 872 the transcriptional regulator CCAAT/enhancer binding protein δ ', *Proceedings of the National*
873 *Academy of Sciences of the United States of America*, 95(18), pp. 10908–10913. doi:
874 10.1073/pnas.95.18.10908.
- 875 Vogl, T. *et al.* (2007) 'Mrp8 and Mrp14 are endogenous activators of Toll-like receptor 4,
876 promoting lethal, endotoxin-induced shock.', *Nature medicine*, 13(9), pp. 1042–1049. doi:
877 10.1038/nm1638.
- 878 Vogl, T. *et al.* (2014) 'Alarmin S100A8/S100A9 as a biomarker for molecular imaging of local
879 inflammatory activity', *Nature Communications*, 5(May), pp. 1–12. doi:
880 10.1038/ncomms5593.
- 881 Vogl, T. *et al.* (2018) 'Autoinhibitory regulation of S100A8/S100A9 alarmin activity locally
882 restricts sterile inflammation', *Journal of Clinical Investigation*, 128(5), pp. 1852–1866. doi:
883 10.1172/JCI89867.
- 884 Wadleigh, D. J. *et al.* (2000) 'Transcriptional activation of the cyclooxygenase-2 gene in
885 endotoxin- treated RAW 264.7 macrophages', *Journal of Biological Chemistry*. © 2000
886 ASBMB. Currently published by Elsevier Inc; originally published by American Society for
887 Biochemistry and Molecular Biology., 275(9), pp. 6259–6266. doi: 10.1074/jbc.275.9.6259.
- 888 Wang, G. G. *et al.* (2006) 'Quantitative production of macrophages or neutrophils ex vivo
889 using conditional Hoxb8.', *Nature methods*, 3(4), pp. 287–293. doi: 10.1038/nmeth865.
- 890 Wang, J. M. *et al.* (2006) 'Functional role of NF-IL6 β and its sumoylation and acetylation
891 modifications in promoter activation of cyclooxygenase 2 gene', *Nucleic Acids Research*,
892 34(1), pp. 217–231. doi: 10.1093/nar/gkj422.
- 893 Wang, Q. *et al.* (2021) 'A hierarchical and collaborative BRD4/CEBPD partnership governs
894 vascular smooth muscle cell inflammation', *Molecular Therapy - Methods and Clinical*
895 *Development*. Elsevier Ltd., 21(June), pp. 54–66. doi: 10.1016/j.omtm.2021.02.021.
- 896 Whiddon, J. L. *et al.* (2017) 'Conservation and innovation in the DUX4-family gene network',

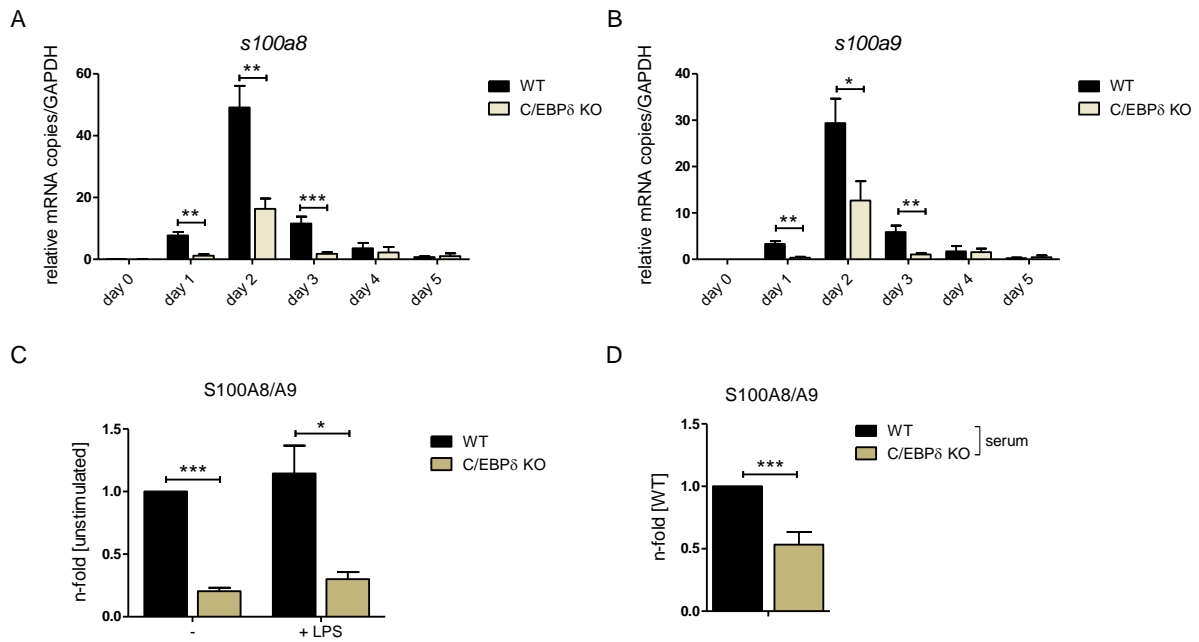
- 897 *Nature Genetics*, 49(6), pp. 935–940. doi: 10.1038/ng.3846.
- 898 Xiang, Y. *et al.* (2007) 'JMJD3 is a histone H3K27 demethylase', *Cell Research*, 17(10), pp.
899 850–857. doi: 10.1038/cr.2007.83.
- 900 Xu, Y. *et al.* (2018) 'A TFIID-SAGA Perturbation that Targets MYB and Suppresses Acute
901 Myeloid Leukemia', *Cancer Cell*. Elsevier Inc., 33(1), pp. 13-28.e8. doi:
902 10.1016/j.ccell.2017.12.002.
- 903 Yang, Q. *et al.* (2017) 'IRF7 regulates the development of granulocytic myeloid-derived
904 suppressor cells through S100A9 transrepression in cancer', *Oncogene*, (October 2016), pp.
905 1–12. doi: 10.1038/onc.2016.448.
- 906 Zenz, R. *et al.* (2007) 'Activator protein 1 (Fos/Jun) functions in inflammatory bone and skin
907 disease', *Arthritis Research & Therapy*, 10(1), p. 201. doi: 10.1186/ar2338.
- 908 Zhang, Y. *et al.* (2008) 'Model-based Analysis of ChIP-Seq (MACS)', *Genome Biology*, 9(9),
909 p. R137. doi: 10.1186/gb-2008-9-9-r137.
- 910

911 **MAIN FIGURES**



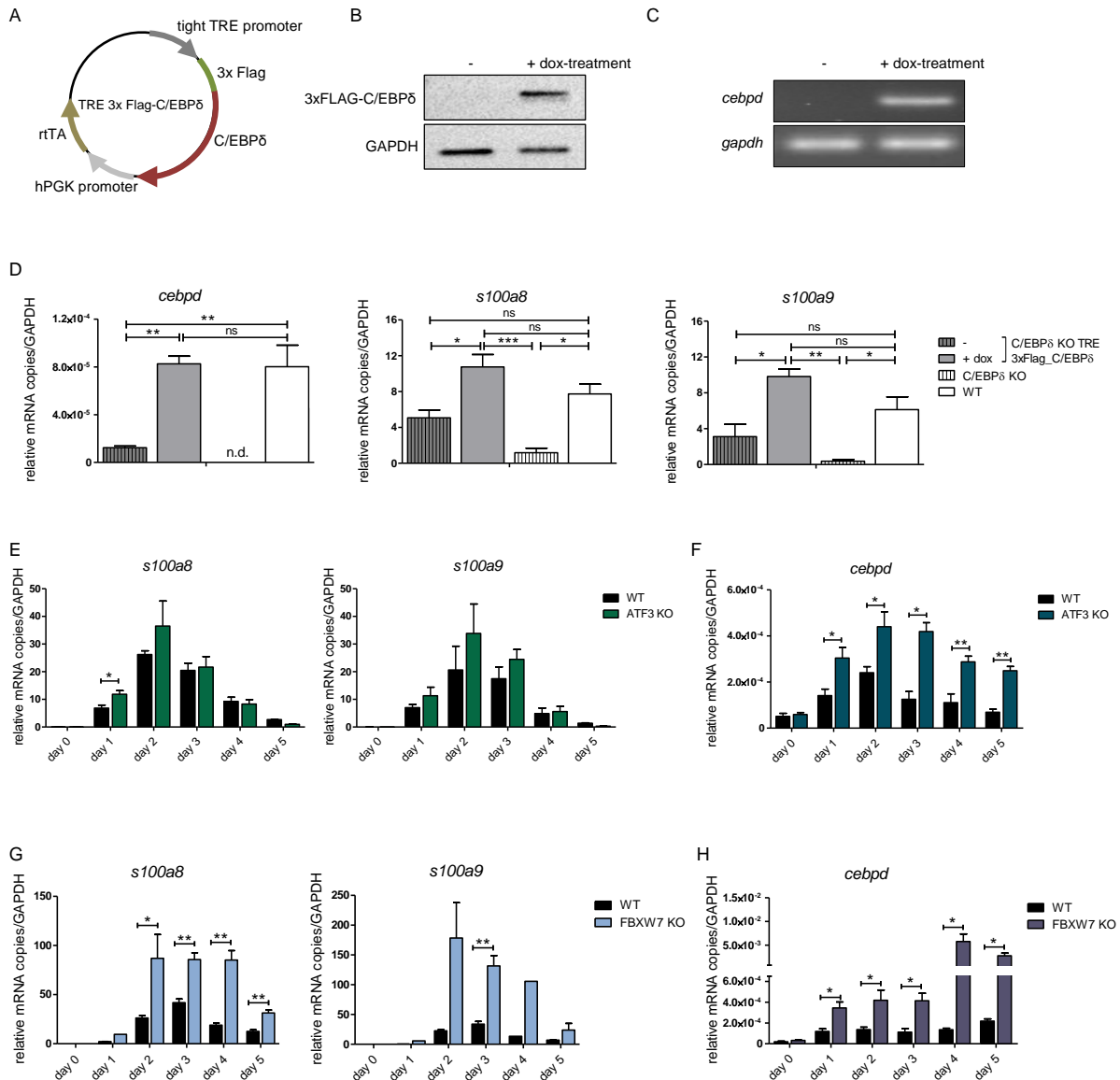
912

913 **Figure 1: Genome-Scale CRISPR Knockout lentiviral pooled library screen to identify**
 914 **S100A9-regulators.** (A) For genome-wide screen, over 100,000 plasmids, each containing a
 915 guide RNA towards different early consecutive exons, were packaged into lentiviral particles.
 916 Cas9 expressing ER-Hoxb8 cells were pool-transduced, selected and differentiated to induce
 917 S100A9 expression. Hits and reference cells were collected by sorting according to their
 918 phenotypes of interest. DNA of both samples was purified for next-generation sequencing
 919 and subsequent analysis. (B) Precursor and differentiated Cas9 and Cas9-library ER-Hoxb8
 920 cells were stained intracellularly for S100A9 using a FITC-labelled antibody. Cas9-library ER-
 921 Hoxb8 day 3 monocytes with no or lower S100A9 expression were sorted as hits, the
 922 remaining cells served as reference cells. (C) Data was analysed using the MAGeCK
 923 software for identification of enriched guide RNAs in the hit sample. Corresponding genes
 924 were rank-ordered by robust rank aggregation (RRA) scores. The list states the top 20 genes
 925 according to RRA scores, arranged after the number of guides that are enriched in the hit
 926 sample



927

928 **Figure 2: Figure 3: S100A8 and S100A9 expression in WT and C/EBPδ KO ER-Hoxb8**
929 **monocytes.** (A) Relative s100a8 and (B) s100a9 mRNA levels were measured using qRT-
930 PCR (n = 3-8). (C) S100A8/A9 concentrations in supernatant of differentiation day 4 of WT
931 and C/EBPδ KO monocytes stimulated with 10 ng LPS for 4 hours or left untreated (n = 3)
932 and (D) serum concentrations of S100A8/A9 in WT and C/EBPδ KO mice were quantified
933 using our in-house mouse S100A8/S100A9 sandwich ELISA (n = 6). Values are the means ±
934 SEM. *P < 0.05, **P < 0.01, ***P < 0.001, by two-tailed Student's t test. See also Figure
935 supplements 1, 2, and 3.



936

937 **Figure 3: Figure 4: S100A8 and S100A9 expression in differentiated ER-Hoxb8 cells is**

938 **dependent on C/EBPδ abundance.** (A) Tet-On construct of inducible 3xFlag-C/EBPδ

939 expression due to constitutively expressed rtTA (reverse tetracycline-controlled

940 transactivator) that binds to TRE promoter upon doxycycline-treatment was transduced into

941 C/EBPδ KO ER-Hoxb8 cells. (B) Induction of 3xFlag-C/EBPδ upon doxycycline treatment (2

942 μg/mL, 24h) was analysed by western blot and (C) qRT-PCR in comparison to untreated

943 cells. (D) Induction of 3xFlag-C/EBPδ was also analysed by qRT-PCR (*cebpd*), as well as

944 expression of *s100a8* and *a9* mRNAs, in untreated and dox-treated C/EBPδ KO

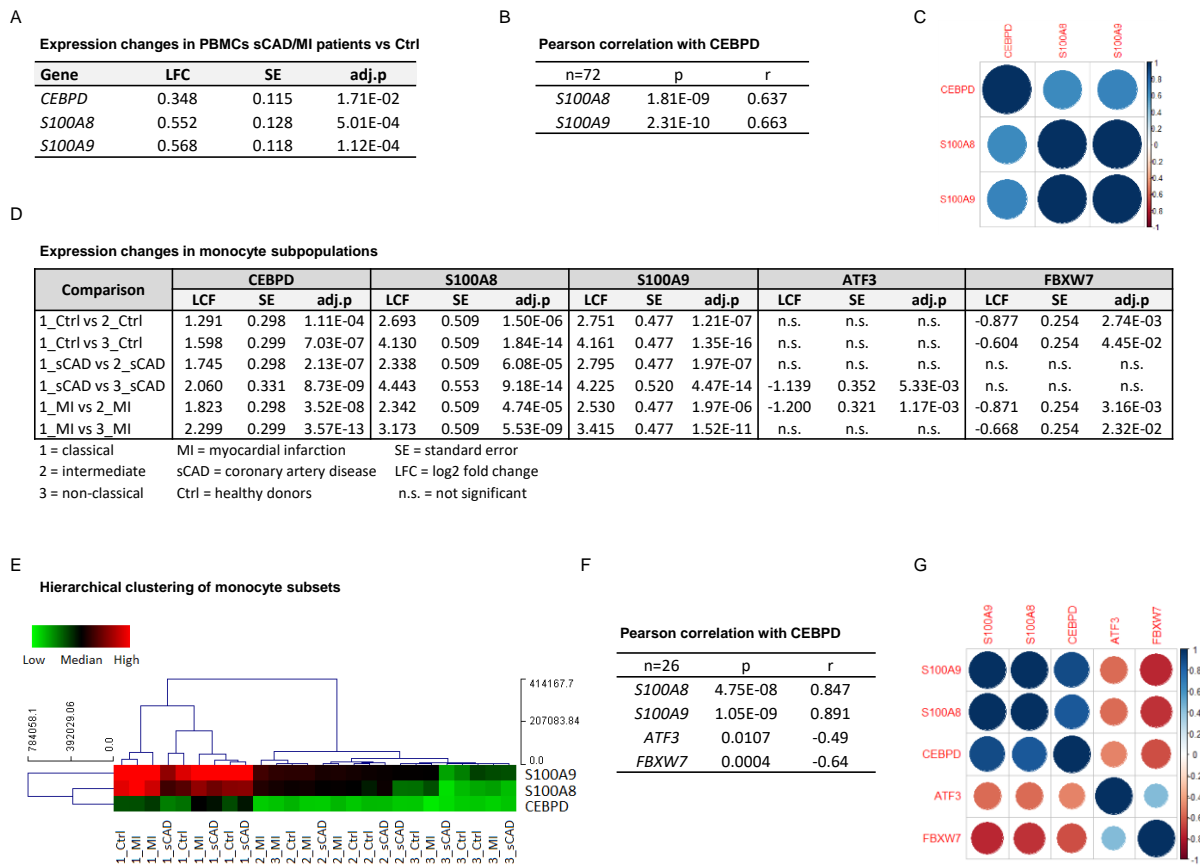
945 TRE_3xFlag-C/EBPδ monocytes and in comparison to WT and C/EBPδ KO monocytes on

946 differentiation day 1 (n = 3). (E, G) S100a8 and s100a9, (F, H) and *cebpd* mRNA levels were

947 measured using qRT-PCR in precursor and differentiated WT and ATF3 KO (E, F) and in WT

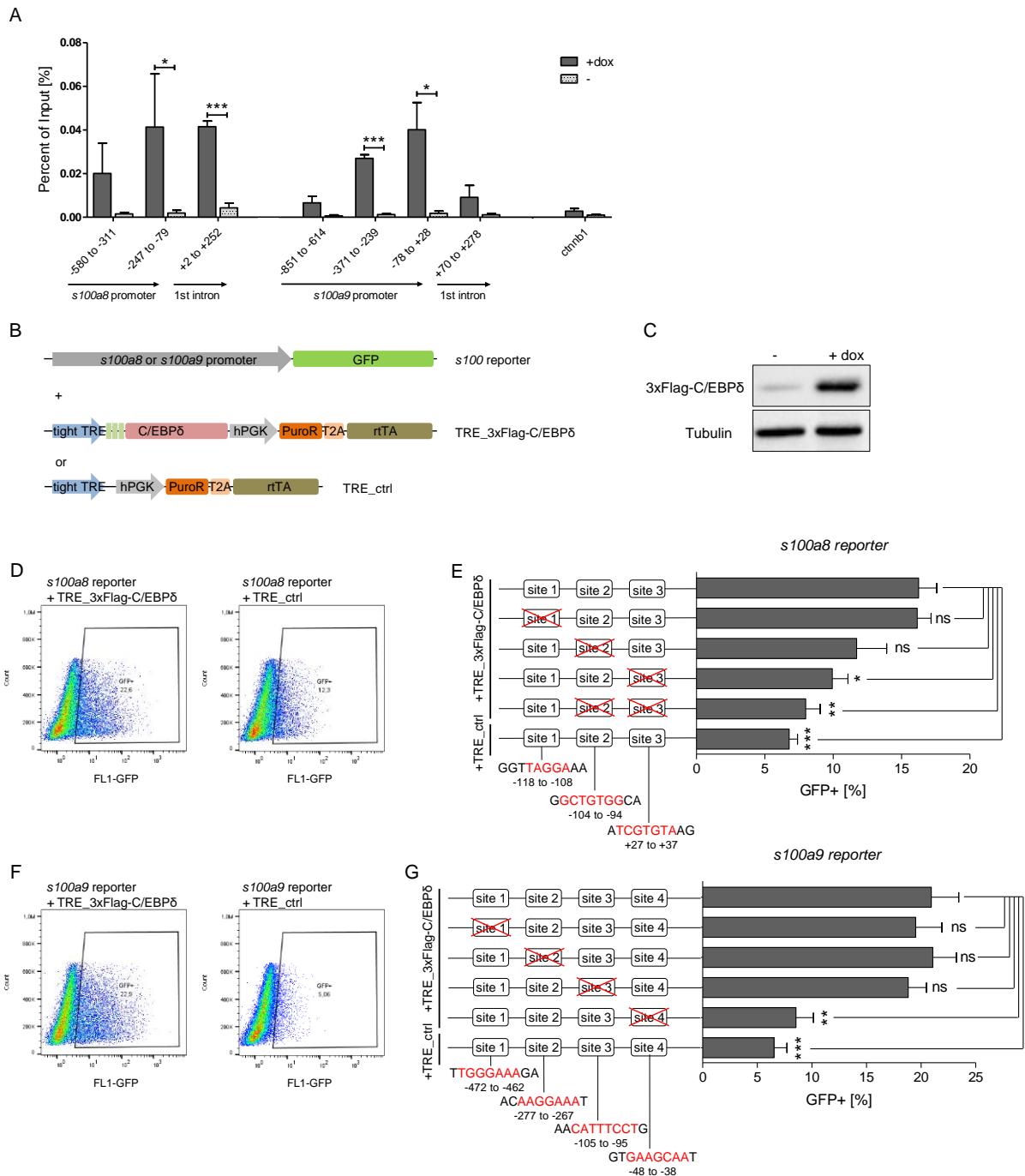
948 and FBXW7 KO (G, H) ER-Hoxb8 monocytes (n = 3-4). Values are the means ± SEM. *P <

949 0.05, **P < 0.01, by one-way ANOVA with Bonferroni correction (D) and by two-tailed
950 Student's t test (E-H).



951

952 **Figure 4: C/EBP δ expression positively correlates with S100A8 and S100A9**
953 **expression in proinflammatory monocytes of MI/sCAD patients.** (A) Gene expression
954 changes detected by RNA-seq in PBMCs of BioNRW participants (n=72, sCAD/MI vs Ctrl).
955 LFC = log2 fold change, SE = standard error, and adj.p = adjusted P-value. (B) Pearson
956 correlation coefficient = r, P-value = p in PBMCs and (C) corresponding correlation matrix.
957 (D) Gene expression changes of *CEBPD*, *S100A8*, *S100A9*, *ATF3* and *FBXW7* detected by
958 RNA-seq in monocyte subpopulations of BioNRW participants (n=26, from 3 individuals in
959 each of the sCAD, MI and Ctrl diagnostic groups). (E) Hierarchical clustering of *S100A8*-,
960 *S100A9*- and *CEBPD* normalised counts (using Euclidean distance metric with complete
961 linkage). Shown are classical (1), intermediate (2) and non-classical (3) monocytes of healthy
962 donors (Ctrl), myocardial infarction (MI) and stable coronary artery disease (sCAD) patients.
963 (F) Pearson correlation coefficient = r, P-value = p in monocytes and (G) corresponding
964 correlation matrix. See also Supplementary Table S9.

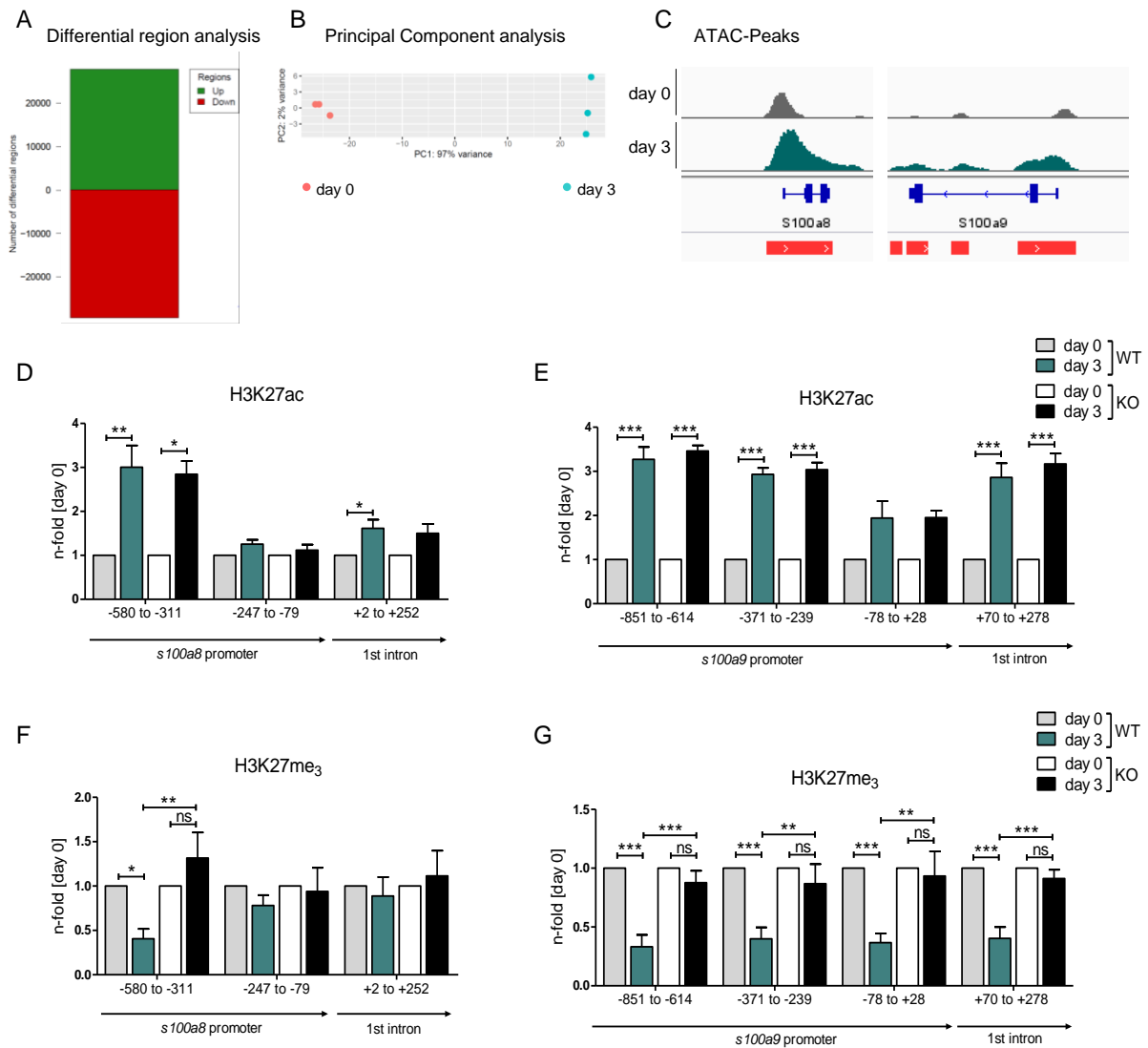


965

966 **Figure 5: C/EBPδ binds to regions within the *s100a8* and *s100a9* promoters.** (A)
 967 Chromatin immunoprecipitation was performed in untreated (-) and dox-treated (+dox)
 968 TRE_3xFlag-C/EBPδ monocytes on differentiation day 1 using a Flag-antibody. Purified DNA
 969 was analysed using primer pairs flanking different *s100a8* and *s100a9* promoter and intronic
 970 regions and a negative control primer pair flanking a random genomic region (n = 3). (B) Co-
 971 transfection of vectors carrying constructs for GFP under the *s100a8* or *s100a9* promoter
 972 (reporter), together with the doxycycline-dependent 3xFlag-C/EBPδ expression cassette
 973 (TRE_3xFlag-C/EBPδ) or a corresponding control vector lacking the 3xFlag-C/EBPδ

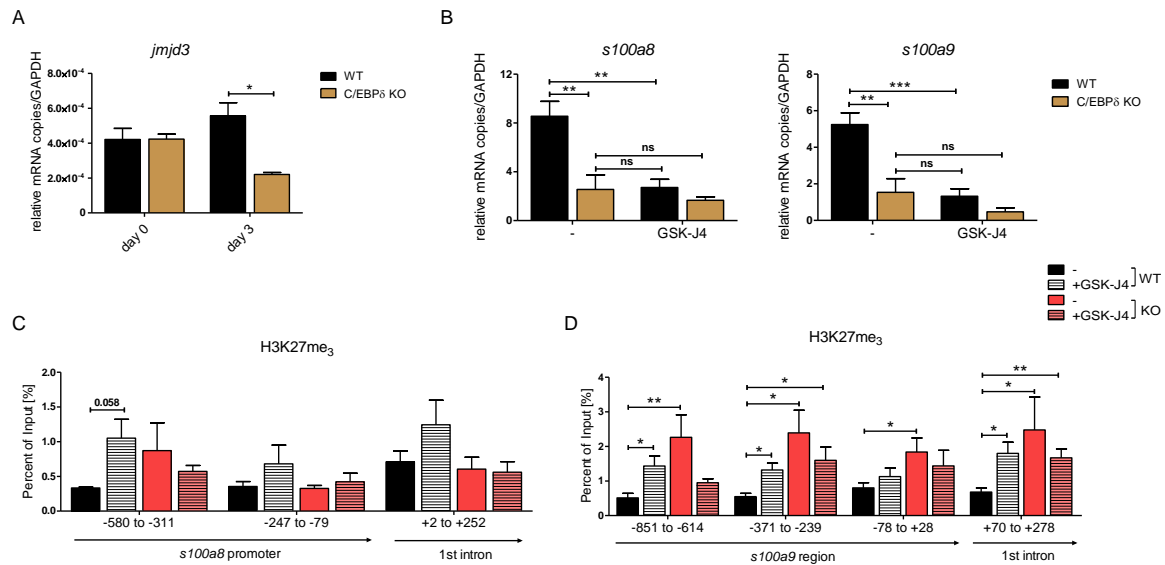
974 expression cassette (TRE_ctrl) in HEK293T cells, was performed. (C) Induction of 3xFlag-
975 C/EBP δ upon doxycycline treatment (2 μ g/mL, 24h) was analysed by western blot.
976 Representative dot plots from flow cytometry analysis show GFP+ gates of co-transfected
977 HEK293T cells, either using TRE_3xFlag-C/EBP δ or TRE_ctrl together with *s100a8* reporter
978 (D) and with *s100a9* reporter (F) upon doxycycline treatment (2 μ g/mL, 24h). Co-transfection
979 of TRE_3xFlag-C/EBP δ and *s100a8* (E) and *s100a9* (G)-reporter plasmids carrying different
980 mutated possible binding sites was performed, analysed 24h post-transfection and compared
981 to co-transfection of TRE_ctrl and s100-reporter plasmid activities. Suggested C/EBP binding
982 sites targeted by depletion are indicated by nucleic acids marked in red (n = 4-5). Values are
983 the means \pm SEM. *P < 0.05, **P < 0.01, ***P < 0.001, ns = not significant, by two-tailed
984 Student's t test.

985



986

987 **Figure 6: Analysis of chromatin accessibility and epigenetic features within *s100a8***
 988 **and *s100a9* promoter regions.** ATAC sequencing (ATAC-seq) was executed in precursor
 989 (day 0) and differentiated (day 3) WT ER-Hoxb8 monocytes. (A) Differential region analysis
 990 and (B) principal component analysis (PCA) were performed ($n = 3$). (C) Representative
 991 gene tracks showing ATAC-seq reads of precursor (day 0) and differentiated (day 3) cells at
 992 the *s100a8* and *s100a9* gene regions. Red bars beneath genomic locations mark regions
 993 with significantly increased ATAC-signals in day 3 samples compared to day 0 samples.
 994 Chromatin-Immunoprecipitation was performed using anti-H3K27ac (D, E), anti-H3K27me₃
 995 (F, G) in chromatin of precursor (day 0) and differentiated (day 3) WT and C/EBP δ KO (KO)
 996 ER-Hoxb8 monocytes. Purified DNA was analysed using primer pairs flanking different
 997 *s100a8* (D, F) and *s100a9* (E, G) promoter regions ($n = 3-6$). N-folds are based on percent of
 998 input-values of respective day 0 ChIP-PCR samples. Values are the means \pm SEM.
 999 * $P < 0.05$, ** $P < 0.01$, *** $P < 0.001$, ns = not significant, by one-way ANOVA with Bonferroni
 1000 correction.



1001

1002 **Figure 7: JMJD3-mediated demethylation of H3K27me₃ is crucial for *s100a8* and**
 1003 ***s100a9* expression.** (A) *Jmjd3* mRNA levels of precursor and differentiated WT and C/EBP δ
 1004 KO ER-Hoxb8 cells were analysed using qRT-PCR (n = 3). (B) WT and C/EBP δ KO ER-
 1005 Hoxb8 cells were treated with 5 μ M GSK-J4 for 3 days during differentiation and *s100a8* and
 1006 *s100a9* mRNA levels were analysed using qRT-PCR (n = 5). Chromatin-Immunoprecipitation
 1007 was performed using anti-H3K27me₃ and appropriate IgG control antibodies in chromatin of
 1008 vehicle controls (-) and treated (+GSK-J4) WT and C/EBP δ KO (KO) ER-Hoxb8 monocytes.
 1009 Purified DNA was analysed using primer pairs flanking different *s100a8* (C) and *s100a9* (D)
 1010 promoter regions (n = 3-5). Values are the means \pm SEM. *P < 0.05, **P < 0.01, ***P <
 1011 0.001, ns = not significant, by one-way ANOVA with Bonferroni correction (A, B) or by two-
 1012 tailed Student's t test in comparison to WT (-) (C, D).

1013

1014

1015 **SUPPLEMENTAL ITEMS**

1016 **FIGURES**

1017 Figure 2 – figure supplement 1: S100A8, S100A9 and C/EBP δ -expression kinetics in ER-
1018 Hoxb8 cells.

1019 Figure 2 – figure supplement 2: Functional properties of WT and C/EBP δ KO ER-Hoxb8
1020 monocytes.

1021 Figure 2 – figure supplement 3: Relative S100A8 and S100A9 expression in differentiated
1022 single KO ERHoxb8 monocytes.

1023 **TABLES**

1024 Table S1: Gene summary of MaGECK analysis (related to main Figure 1)

1025 Table S2: List of guides (stated in 5'-3' orientation) for cloning into lentiCRISPR v2, related to
1026 Methods

1027 Table S3: List of primer (stated in 5'-3' orientation) for amplifying GeCKO library and NGS,
1028 related to Methods

1029 Table S4: List of oligonucleotides (stated in 5'-3' orientation, fw: forward, rv: reverse) for
1030 cloning steps to construct TRE_3xFlag-C/EBP δ vector, related to Methods

1031 Table S5: List of oligonucleotides (stated in 5'-3' orientation, fw: forward, rv: reverse) for
1032 cloning steps to construct s100a8 and s100a9 reporter construct, related to Methods

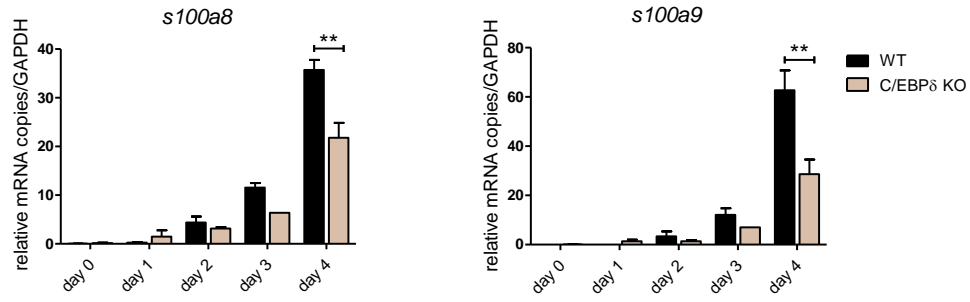
1033 Table S6: List of oligonucleotides (stated in 5'-3' orientation) for mutagenesis to disrupt
1034 specific sites within s100a8 and s100a9 reporter vectors, related to Methods

1035 Table S7: List of qRT-PCR primer (in 5'-3' orientation) used for qRT-PCR, related to Methods

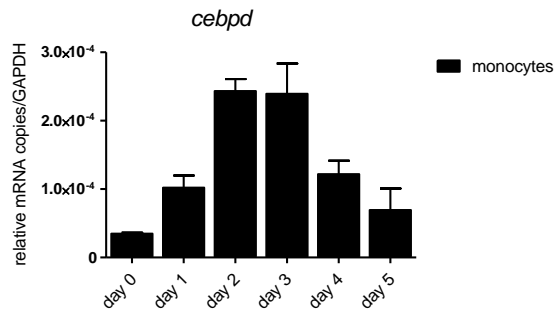
1036 Table S8: List of CHIP-PCR primer (in 5'-3' orientation) for s100a8 and s100a9 genomic
1037 locations, related to Methods

1038 Table S9: Expression changes in the BioNRW monocytes dataset (RNA-seq, n=26) (related
1039 to main Figure 4)

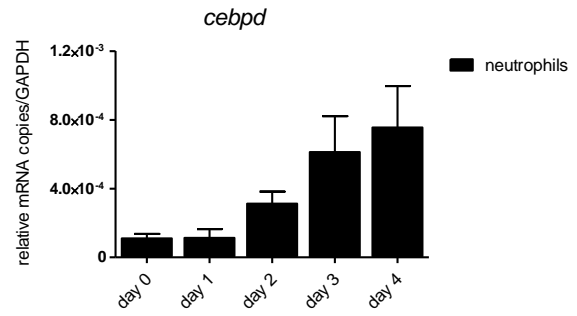
A



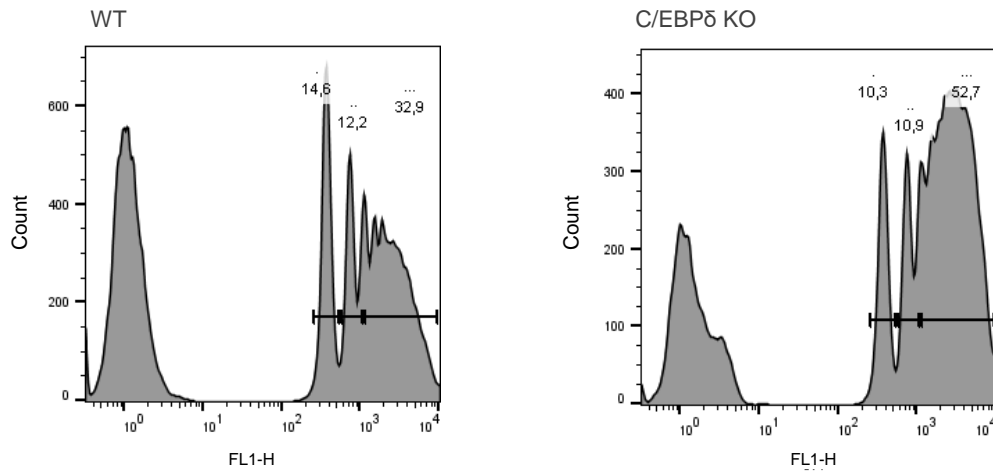
B



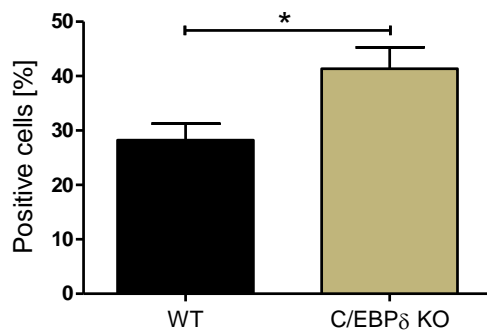
C



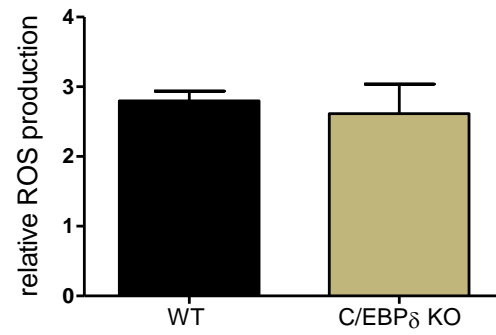
A



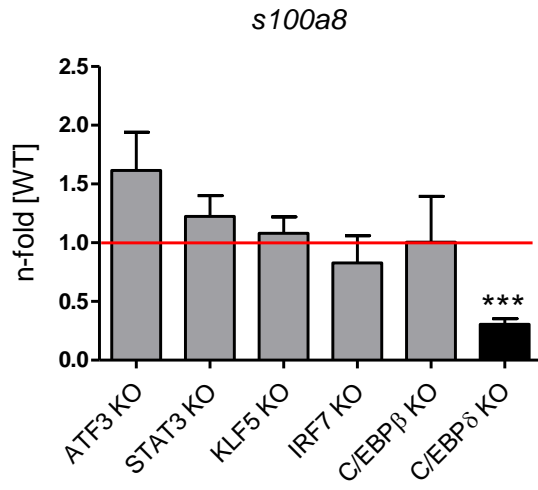
B



C



A



B

